Measurements of Hydrodynamic Forces on the Impeller of the HPOTP of the SSME

by

Ron Franz and Norbert Arndt

California Institute of Technology
Division of Engineering and Applied Science
Pasadena, California 91125

March 1986

Report Number E249.2

Contract NAS 8-33108
Approved: A.J. Acosta
C.E. Brennen
T.K. Caughey

NOMENCLATURE

[A]	hydrodynamic force matrix, non-dimensionalized by $\rho\pi\omega^2 r_2^2 b_2$
A_2	impeller outlet area ($2\pi r_2 b_2$)
b_2	impeller discharge width (0.57 in)
{F}	6-component generalized force vector
F_1, F_2	components of the instantaneous lateral force on the impeller in the rotating dynamometer reference frame
F_x, F_y	components of the instantaneous lateral force on the impeller in the fixed laboratory reference frame (X,Y), non-dimensionalized by $\rho\pi\omega^2 r_2^3 b_2$
F_{ox}, F_{oy}	values of F_x and F_y if the impeller was located at the the origin of the (X,Y) coordinate system (volute center), non-dimensionalized by $\rho\pi\omega^2 r_2^3 b_2$
F_N, F_T	components of the lateral force on the impeller normal to and tangential to the whirl orbit, averaged over the orbit, non-dimensionalized by $\rho\pi\omega^2 r_2^2 b_2 \varepsilon$
I/J	ratio of whirl/main shaft speed
P_{t1}, P_{t2}	upstream, downstream total pressure

Q flow rate

r_2 impeller discharge radius (3.3 in.)

T shaft torque

t time

(X,Y) fixed laboratory reference frame

x,y instantaneous coordinates of the impeller center in the fixed laboratory reference frame (X,Y), non-dimensionalized by r_2

ε radius of the circular whirl orbit

η impeller efficiency, $Q(p_{t2} - p_{t1})/(T\omega)$

θ angle of the impeller on the eccentric circle, measured from the volute tongue in the direction of impeller rotation

ρ density of water

ϕ flow coefficient based on the impeller discharge area and tip speed, $\frac{Q}{\omega r_2 A_2}$

Ψ total head coefficient, $\frac{p_{t2} - p_{t1}}{\rho \omega^2 r_2^2}$

ω radian frequency of the impeller (shaft) rotation

Ω radian frequency of the whirl motion = $I\omega/J$

1. Introduction

The references [1-4] provide a complete description of the facility. Briefly, the dynamometer, composed of two parallel plates connected by four strain gaged posts, is mounted between the impeller and the drive shaft. It measures the six components of a generalized hydrodynamic force vector {F} acting on the impeller. The impeller can be subject to whirling motion in an orbit eccentric to the volute center, in addition to the normal impeller rotation. Since the eccentric motion is in the lateral plane, perpendicular to the impeller centerline, only the two components of the force vector {F} in this lateral plane will be discussed.

Refering to Fig. 1, these forces, in the volute frame of reference, can be represented by

$$\begin{Bmatrix} F_x \\ F_y \end{Bmatrix} = \begin{Bmatrix} F_{ox} \\ F_{oy} \end{Bmatrix} + [\, A\ (\Omega/\omega)\,] \begin{Bmatrix} \varepsilon/r2\ \cos\Omega t \\ \varepsilon/r2\ \sin\Omega t \end{Bmatrix} \tag{1}$$

The lateral forces, represented by F_x and F_y, can be considered as the sum of two forces: a fixed force, represented by F_{ox} and F_{oy}, which the impeller would experience if located at the volute center, and an unsteady force due to the eccentric motion of the impeller, represented by a force matrix [A]. The gravitational and bouyancy forces on the rotor are subtracted out. Dimensionless quantities are used throughout (see Nomenclature for definitions).

Hydraulic performance curves ($\Psi\ (\phi)$), efficiency curves ($\eta\ (\phi)$), the steady force and the hydrodynamic force matrix [$A(\Omega/\omega)$] were measured using the impeller of the HPOTP of the SSME (referred to as Impeller R). Three different impeller/volute combinations were investigated,

-Impeller R/Volute E

(a vaned diffuser with 17 vanes and elliptical cross section)

This combination was tested for two different radial gap clearances and after the opening up of the radial gap. For a description of the radial gap see paragraph 2 and the enclosed drawing of the test section of the Rotor Force Test Facility (RFTF).

-Impeller R/Volute D

(vaneless diffuser with trapezoidal cross section)

This combination was tested after the opening up of the radial gap.

-Impeller R/no volute

This combination was tested to approximate the case where the impeller is whirling in an infinite medium. It was thus attempted to separate the influence of the volute on the measurements. Except for the shut-off results, these data were were taken after increasing the radial gap by 0.008 inch.

All tests were performed with the face seal clearance set to a minimum of 0.005 inch. The opening of the radial gap did not qualitatively change the results. A strong dependence of the hydrodynamic force matrix on flow coefficient and whirl ratio in all three impeller/volute configurations tested was observed.

2. Modifications of the Test Facility

The RFTF and Impeller R both had to be slightly modified due to the dimensions of Impeller R (inducer diameter and outlet diameter).

The main modification of Impeller R was the reduction of the outlet diameter from 6.85 inch to 6.6 inch, which made it possible to perform experiments on different impeller/volute combinations. Furthermore, some alterations had to be made to the inlet section of the RFTF.

A face seal with seal clearance adjustable from 0.000 inch to 0.120 inch was provided by shrinking a hardened metal ring on the impeller shroud and fastening a ring (metal or Delrin) to the face seal holding device.

Furthermore, initially a radial gap with a clearance, due to the eccentic orbit of the impeller, of 0.005 to 0.105 inch was between the metal ring on the impeller shroud and the face seal holding device. In order to assure that this radial gap would not greatly influence the data to be taken it was first increased by 0.008 inch, and then opened up to a clearance of 0.25 to 0.35 inch.

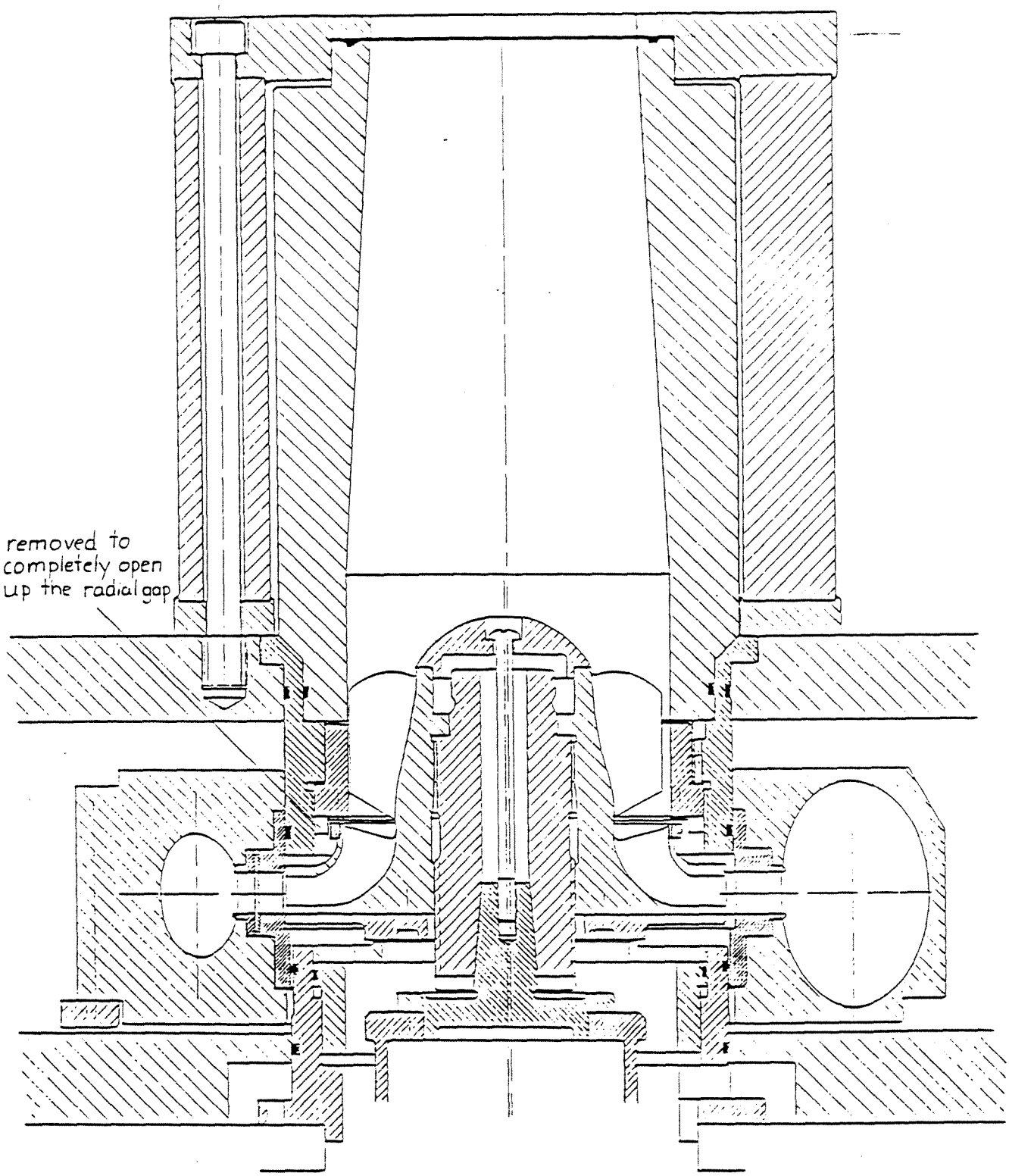

Test Section of the RFTF

3. Performance and Efficiency Tests

Hydraulic performance curves ($\psi(\phi)$) and efficiency curves ($\eta(\phi)$) are presented in figures 2-5 for all three impeller/volute combinations at 1000 rpm and 2000 rpm. The maximum flow rate and the most efficient operating point depended strongly on the volute used. Except for the no volute case, the efficiency increased with increasing rpm whereas the most efficient operating point did not depend significantly on the rotating speed.

TABLE

	Efficiency		Max Flow	Design Flow
	1000 rpm	2000 rpm	1000 rpm	1000 rpm
Volute E	.59	.64	.145	.11
Volute D	.47	.57	.128	.09
no volute	.47	.47	.135	.12

Volute E delivered the highest head at any flow coefficient. For high flow coefficients the head delivered by Volute D was less than the head delivered when no volute was used. Moreover, for low flow coefficients Volute D delivered nearly the same head as Volute E.

4. Steady Forces

Data on the magnitude and the phase of the steady force as a function of flow rate are presented in figures 6-9 for all three combinations, and for the different radial gaps. For Volute D, the magnitude of the steady force has a

minimum as a function of flow coefficient, whereas, for Volute E and no volute there is no significant dependence on flow coefficient, the magnitude for Volute E being smaller than for no volute.

5. Hydrodynamic Force Matrices

All tests to measure the hydrodynamic force matrix $[A(\Omega/\omega)]$ were run at 1000 rpm and at a minimum face seal clearance of 0.005 inch. Examination of the elements of $[A(\Omega/\omega)]$ shows that the diagonal terms are almost equal whereas the off-diagonal terms are almost equal but of opposite sign. This coincides with observations made by B.Jery [2-4] on different impeller/volute combinations. The data on the matrix will be presented in terms of the average normal and tangential force F_N, F_T given by

$$F_N = (A_{xx} + A_{yy})/2 \quad \text{and} \quad F_T = (-A_{xy} + A_{yx})/2$$

Figures 10-21 show F_N and F_T for the three combinations at different flow rates. Note that the data for the no volute case have been taken before the opening of the radial gap. Since this opening did not change significantly the obtained data (as presented later for the Impeller R/Volute E combination) it is justifiable to compare data for all radial gaps.

At the maximum flow rate, for any of the three combinations, the curve of F_T (versus Ω/ω) can be approximated by a straight line (i.e. has approximately constant slope), the region of destabilizing whirl being restricted to $0 < \Omega/\omega < 0.2$. With decreasing flow rate, for both Volute E and Volute D, the curve of F_T changes qualitatively in the same manner. At $\phi=.11$ and $\Omega/\omega=0.1$ an inflection point occurs. At $\phi=0.09$, F_T is approximately constant over a whirl ratio from $-0.1 < \Omega/\omega < 0.4$, and for $\phi < 0.09$ F_T resembles a cubic, the relative minima and

maxima shifted to higher whirl ratios as the flow rate decreases. The region of destabilizing whirl is extended to $\Omega/\omega < 0.6$.

A remarkable effect occurs for Volute E for $\phi < 0.8$. F_T crosses the axis $F_T=0$ three times. Therefore, there exist regions of stabilizing and destabilizing whirl for $0.0 < \Omega/\omega < 0.6$.

In comparison, for the no volute case, the curve of F_T resembles a cubic at higher flow rates ($\phi=0.10$), and the relative minima of F_T do not depend as strongly on whirl ratio.

Figures 22-25 show the transition in the curve of F_T for the different cases.

For all cases investigated, F_N has approximately a parabolic shape.

Figures 26-35 show the effect of opening the radial gap. No noticeable change occured after increasing the gap by 0.008 inch; therefore, no data for that configuration are included in the comparison. Even after opening up the gap completely the shapes of F_N and F_T remained qualitatively similar, and the region of destabilizing whirl ratios was not changed significantly.

For all three impeller/volute combination, tufts were placed in the intake upstream of the inducer. At a position of 0.2 inch upstream of the inducer leading edge, flow reversal was observed for $\phi < 0.095$, independent of volute. For $\phi < 0.075$ flow reversal was observed in a region extending to one inducer diameter upstream of the inducer leading edge.

6. Repeatability

Some repeatability tests were taken, especially in the region of interest, i.e. $0.0 < \Omega/\omega < 0.7$. The scatter in the components of [A], and on F_T and F_N was at most 0.1 , the absolute values of F_T and F_N being < 2 in that particular region. The scatter did not decrease significantly with decreasing magnitude of F_N, F_T . Therefore, the relative error is increasing as the magnitude of F_N, F_T decreases.

7. Conclusions

The impeller of the HPOTP of the SSME was tested at the RFTF at Caltech.

* For a vaneless volute, Volute D, the magnitude of the steady force as a function of flow coefficient showed a distinct minimum. For a vaned diffuser, Volute E, no distinct minimum was observed.
* The magnitude of the tangential force in the region of destabilizing whirl is larger for Impeller R than for any of the impellers (three) tested previously.
* With decreasing flow rate, the shape of the curve F_T versus Ω/ω changed from an approximately straight line at maximum flow rate to a cubic at low flow rates. Simultaneously, the region of destabilizing whirl increased from $\Omega/\omega < 0.2$ to $\Omega/\omega < 0.6$.
* For two volutes with significantly different performances and efficiencies, the transition occurred at about the same flow rate, ϕ=0.09. The impeller tested without volute, the cubic extended to higher flowrates.
* The occurence of flow reversal appears to coincide with the transition of the curve of F_T from a straight line to a cubic.
* Therefore, it is concluded that for high flow rates the effects of the volute dominate the hydrodynamic force matrix [A], whereas for low flow rates the effects of the inducer dominate [A].

REFERENCES

1. Jery, B. and Franz, R., "Stiffness Matrices for the Rocketdyne Diffuser Volute", California Institute of Technology, Div. of Eng. and Appl. Sci., Report No. E249.1, Oct. 1982.

2. Jery, B., Acosta, A.J., Brennen, C.E., and Caughey, T.K., "Hydrodynamic Impeller Stiffness, Damping and Inertia in the Rotordynamics of Centrifugal Pumps," "Third Workshop on Rotordynamic Instability Problems in High Performance Turbomachinery," Texas A&M University, May 28-30,1984.

3. Jery, B., Brennen, C.E., Caughey, T.K., and Acosta, A.J., "Forces on Centrifugal Pump Impellers," "Second International Pump Symposium," Houston, Texas, April 29-May 2,1985.

4. Jery, B., "Experimental Study of Unsteady Hydrodynamic Force Matrices on Whirling Centrifugal Pump-Impellers," Ph.D. Thesis, Division of Engineering and Applied Science, California Institute of Technology, October 1985.

LIST OF FIGURES

Figure 13. Average tangential force for Impeller R at 1000 rpm for ϕ=0.11 with the three volutes. *-radial gap at min. .013 in. clearance.

Figure 14. Average normal force for Impeller R at 1000 rpm for ϕ=0.09 with the three volutes. *-radial gap at min. .013 in. clearance.

Figure 15. Average tangential force for Impeller R at 1000 rpm for ϕ=0.09 with the three volutes. *-radial gap at min. .013 in. clearance.

Figure 16. Average normal force for Impeller R at 1000 rpm for ϕ=0.07 with the three volutes. *-radial gap at min. .013 in. clearance.

Figure 17. Average tangential force for Impeller R at 1000 rpm for ϕ=0.07 with the three volutes. *-radial gap at min. .013 in. clearance.

Figure 18. Average normal force for Impeller R at 1000 rpm for ϕ=0.05 with the three volutes. *-radial gap at min. .013 in. clearance.

Figure 19. Average tangential force for Impeller R at 1000 rpm for ϕ=0.05 with the three volutes. *-radial gap at min. .013 in. clearance.

Figure 20. Average normal force for Impeller R at 1000 rpm for ϕ=0.00 with the three volutes. *-radial gap at min. .013 in. clearance.

Figure 21. Average tangential force for Impeller R at 1000 rpm for ϕ=0.00 with the three volutes. *-radial gap at min. .013 in. clearance.

Figure 22. Transition in the curve of the tangential force for Impeller R at 1000 rpm with Volute E (radial gap at min. .005 in. clearance), showing ϕ=0.11, 0.10, 0.09 and 0.08.

Figure 23. Transition in the curve of the tangential force for Impeller R at 1000 rpm with Volute E (radial gap opened up) for ϕ=0.11, 0.09 and 0.08.

Figure 24. Transition in the curve of the tangential force for Impeller R at 1000 rpm with Volute D for ϕ=0.11, 0.09 and 0.08.

Figure 25. Transition in the curve of the tangential force for Impeller R at 1000 rpm with no volute (radial gap at min. .013 in. clearance), showing ϕ=0.11, 0.10, 0.09 and 0.08.

Figure 26. Comparison of the average normal force for Impeller R/Volute E at 1000 rpm for the radial gap present and opened up at ϕ=0.14. #-radial gap at min. .005 in. clearance.

Figure 27. Comparison of the average tangential force for Impeller R/Volute E at 1000 rpm for the radial gap present and opened up at ϕ=0.14. #-radial gap at min. .005 in. clearance.

Figure 28. Comparison of the average normal force for Impeller R/Volute E at 1000 rpm for the radial gap present and opened up at ϕ=0.11. #-radial gap at min. .005 in. clearance.

Figure 29. Comparison of the average tangential force for Impeller R/Volute E at 1000 rpm for the radial gap present and opened up at ϕ=0.11. #-radial gap at min. .005 in. clearance.

Figure 30. Comparison of the average normal force for Impeller R/Volute E at 1000 rpm for the radial gap present and opened up at ϕ=0.07. #-radial gap at min. .005 in. clearance.

Figure 31. Comparison of the average tangential force for Impeller R/Volute E at 1000 rpm for the radial gap present and opened up at ϕ=0.07. #-radial gap at min. .005 in. clearance.

Figure 32. Comparison of the average normal force for Impeller R/Volute E at 1000 rpm for the radial gap present and opened up at ϕ=0.05. #-radial gap at min. .005 in. clearance.

Figure 33. Comparison of the average tangential force for Impeller R/Volute E at 1000 rpm for the radial gap present and opened up at ϕ=0.05. #-radial gap at min. .005 in. clearance.

Figure 34. Comparison of the average normal force for Impeller R/Volute E at 1000 rpm for the radial gap present and opened up at ϕ=0.00. #-radial gap at min. .005 in. clearance.

Figure 35. Comparison of the average tangential force for Impeller R/Volute E at 1000 rpm for the radial gap present and opened up at ϕ=0.00. #-radial gap at min. .005 in. clearance.

Figures 10-21 of F_N and F_T, comparing the three volutes and Figures 22-25, showing the transition of F_T with flow rate, are repeated with the same Figure #, with a curve drawn through the data points. The drawn curve has no significance other than to connect the data points as an aid in viewing the graph.

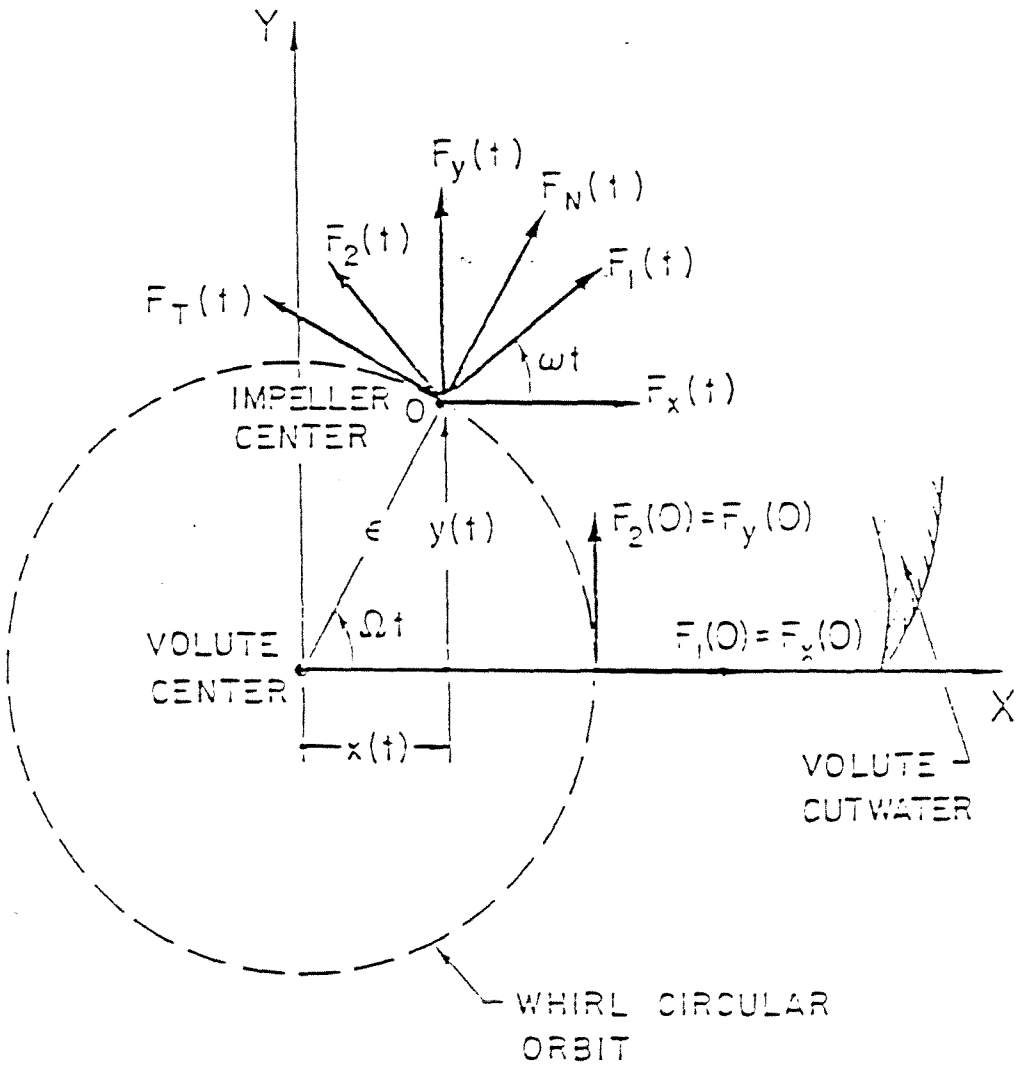

Figure 1. Schematic representing the lateral forces in the rotating dynamometer frame (as F_1, F_2), in the stationary volute frame (as F_x, F_y) and in the local polar coordinate frame (as F_N, F_T).

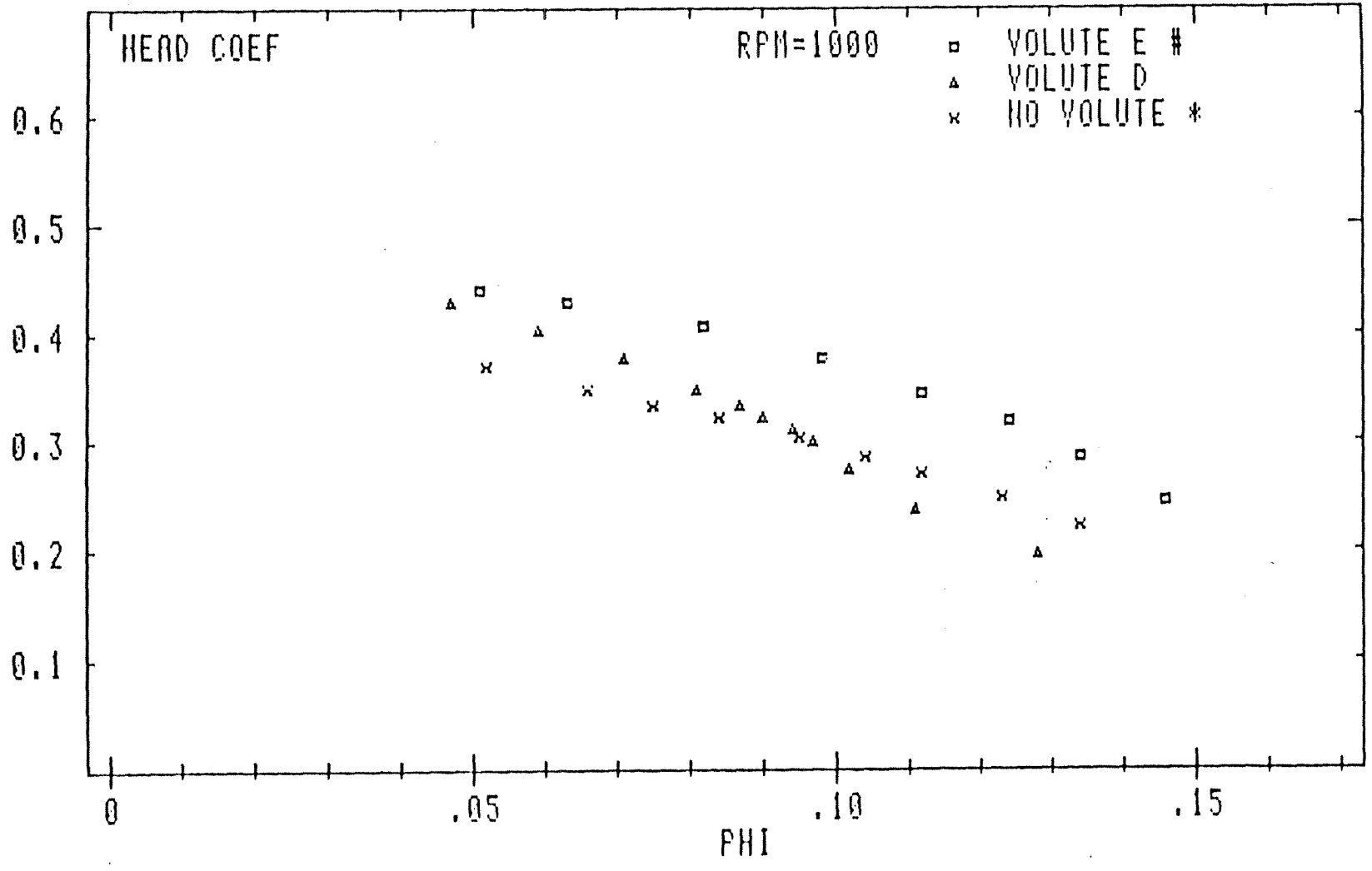
HEAD COEF
RPM=1000
VOLUTE E #
VOLUTE D
NO VOLUTE *
0.6
0.5
0.4
0.3
0.2
0.1
0
.05
.10
.15
PHI

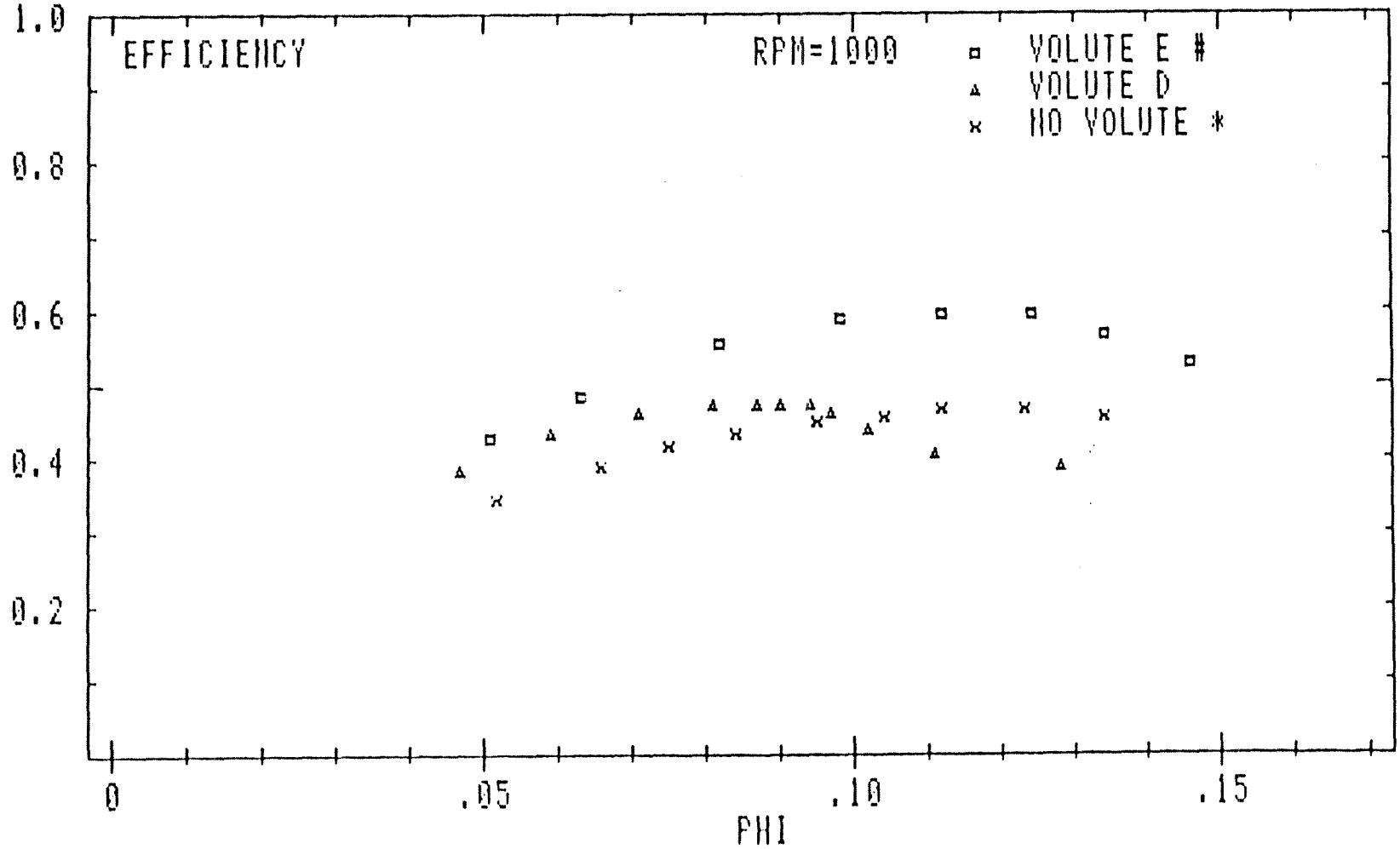
EFFICIENCY
RPM=1000
VOLUTE E #
VOLUTE D
NO VOLUTE *
1.0
0.8
0.6
0.4
0.2
0
.05
.10
.15
PHI

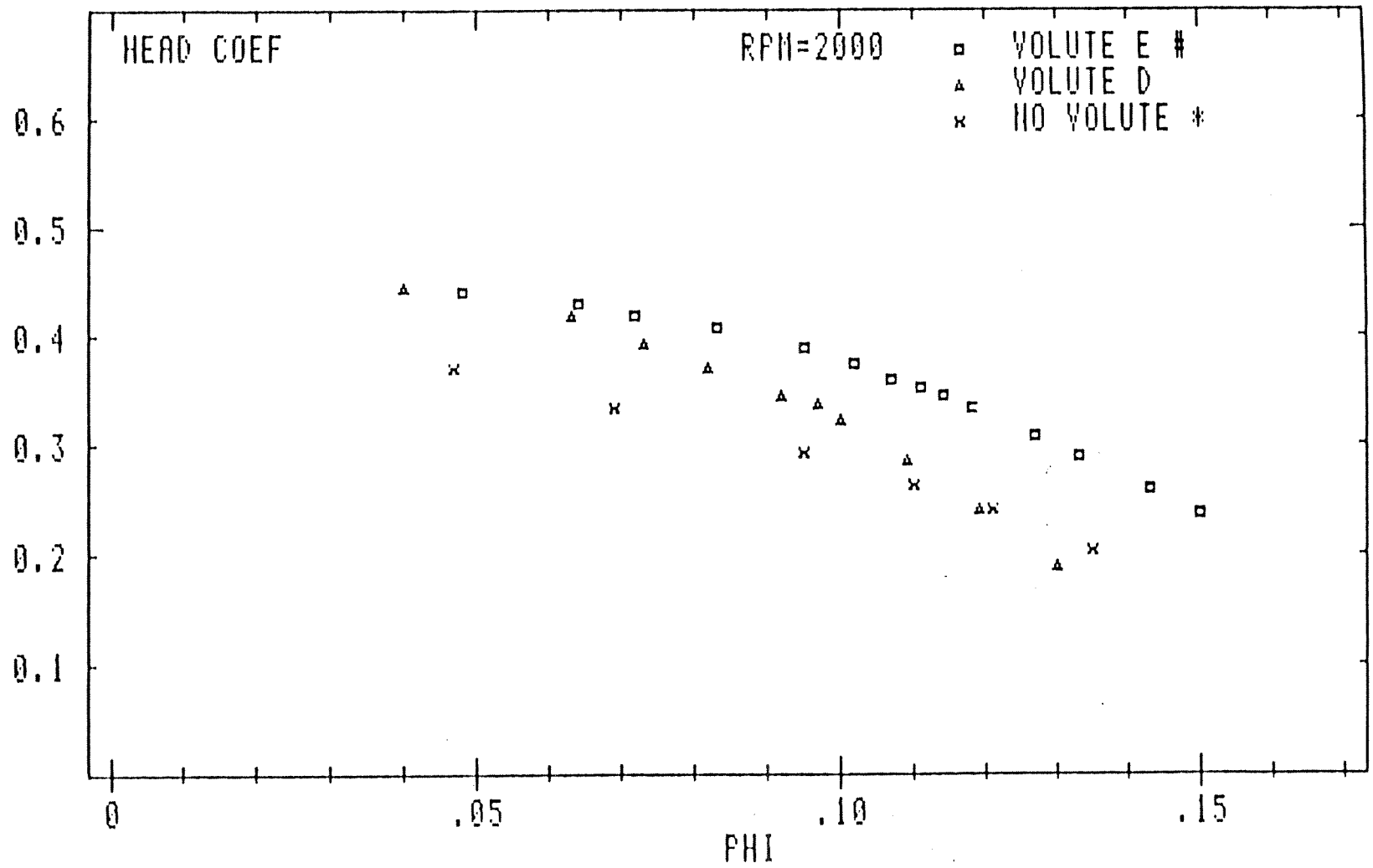
HEAD COEF
RPM=2000
VOLUTE E #
VOLUTE D
NO VOLUTE *
0.6
0.5
0.4
0.3
0.2
0.1
0
.05
.10
.15
PHI

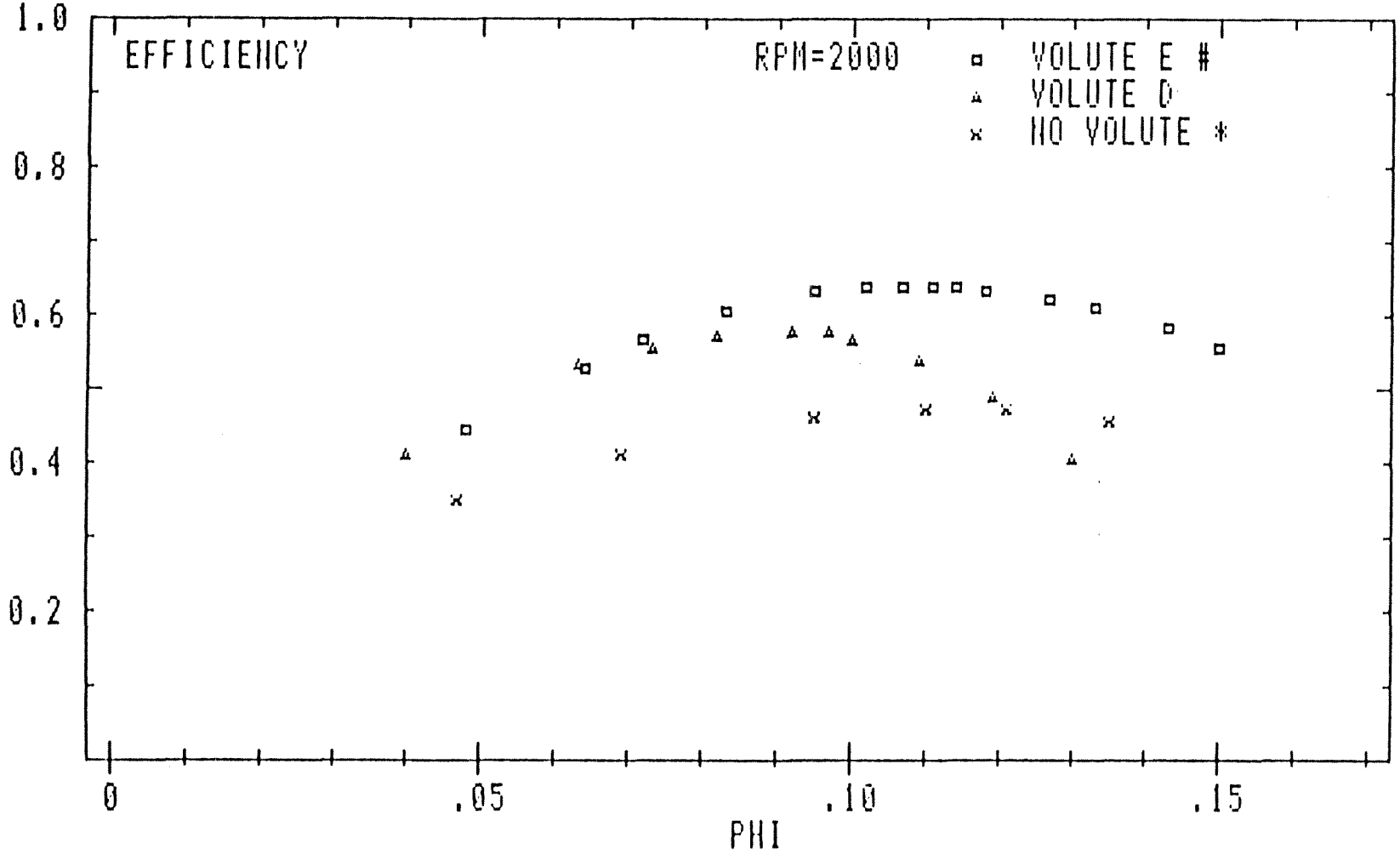
EFFICIENCY
RPM=2000
VOLUTE E #
VOLUTE D
NO VOLUTE *
1.0
0.8
0.6
0.4
0.2
0
.05
.10
.15
PHI

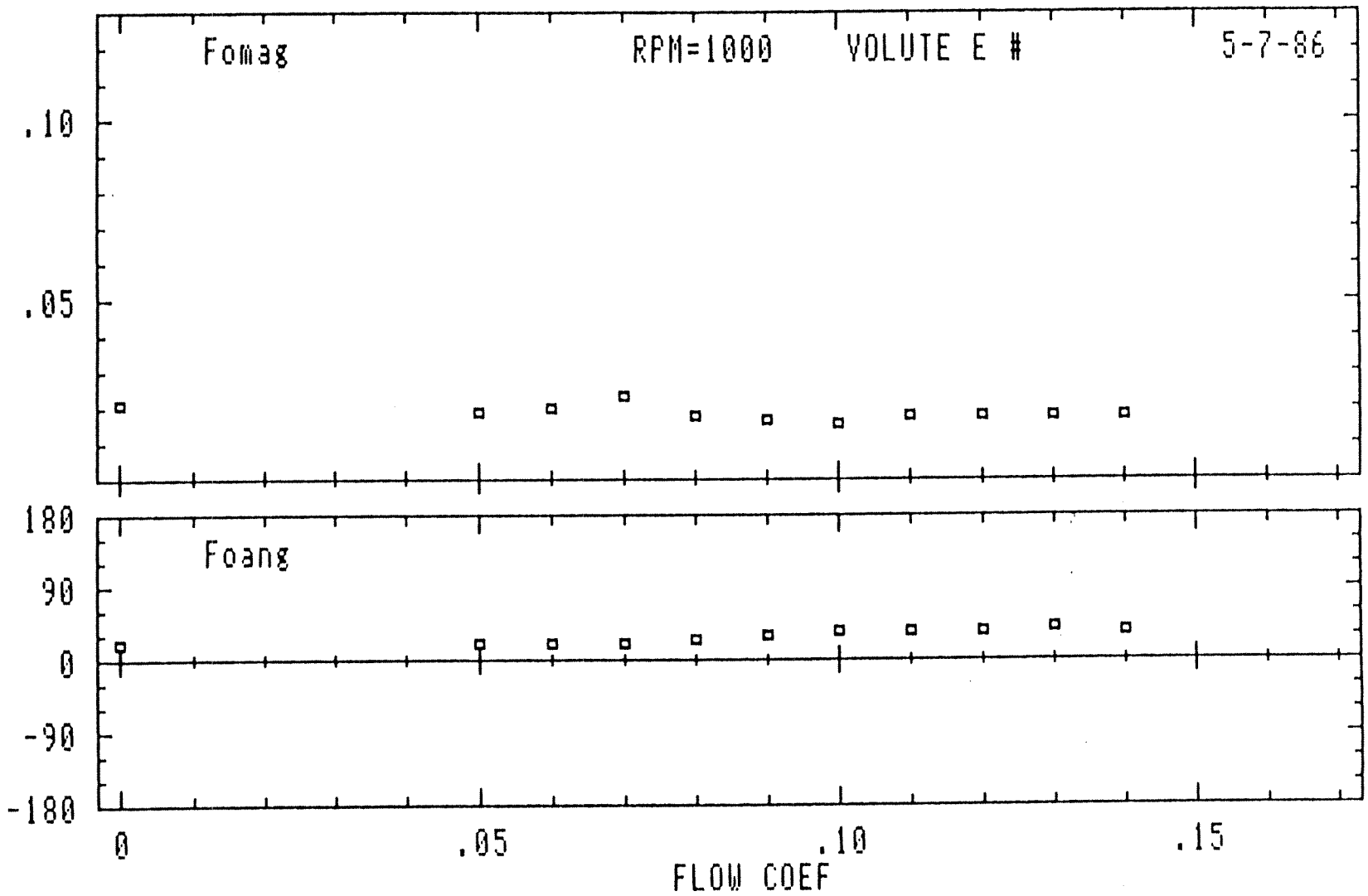
Fomag
RPM=1000
VOLUTE E #
5-7-86
.10
.05
180
90
0
-90
-180
Foang
0
.05
.10
.15
FLOW COEF

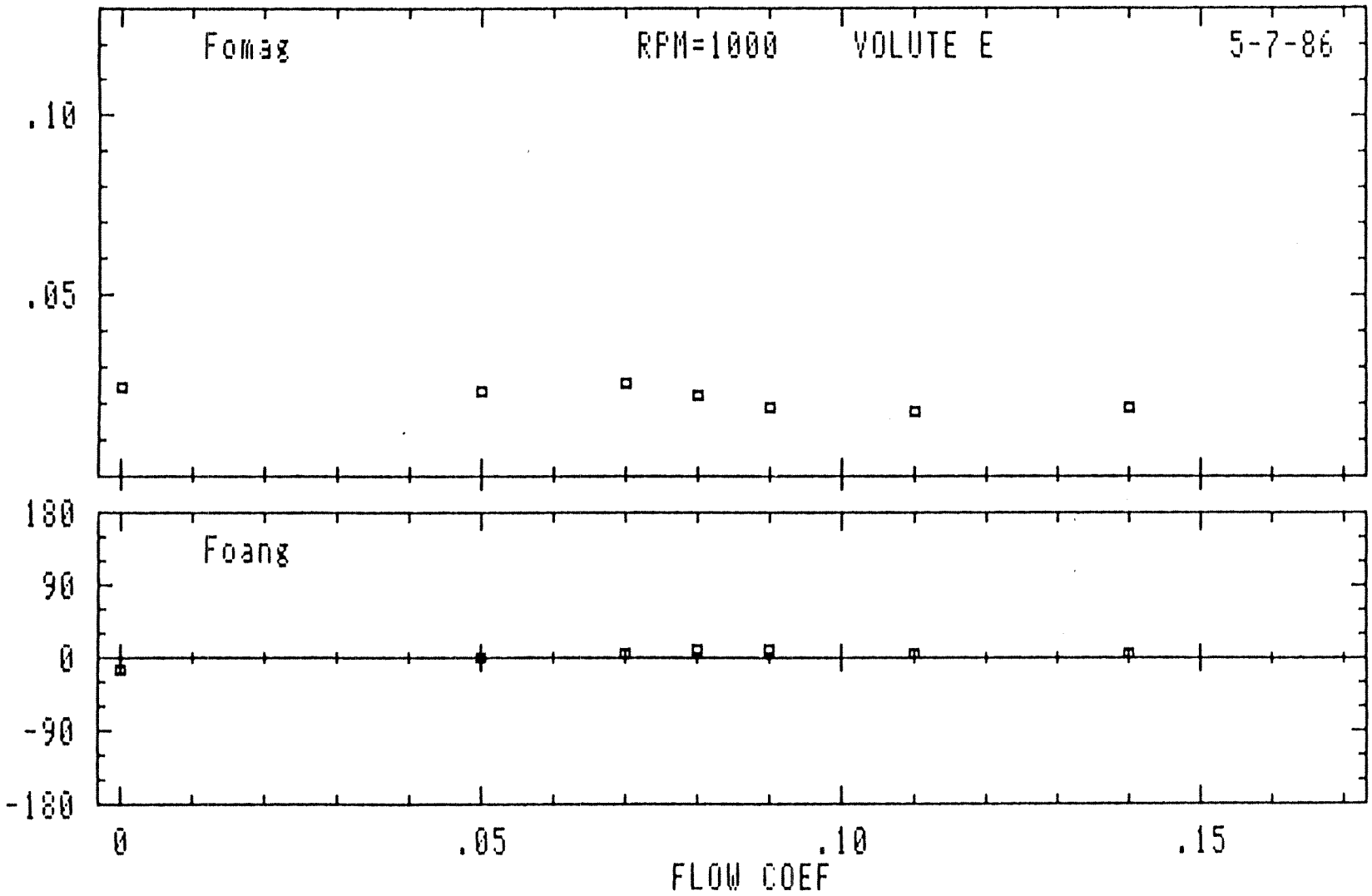
Fomag
RPM=1000
VOLUTE E
5-7-86
.10
.05
180
90
0
-90
-180
Foang
0
.05
.10
.15
FLOW COEF

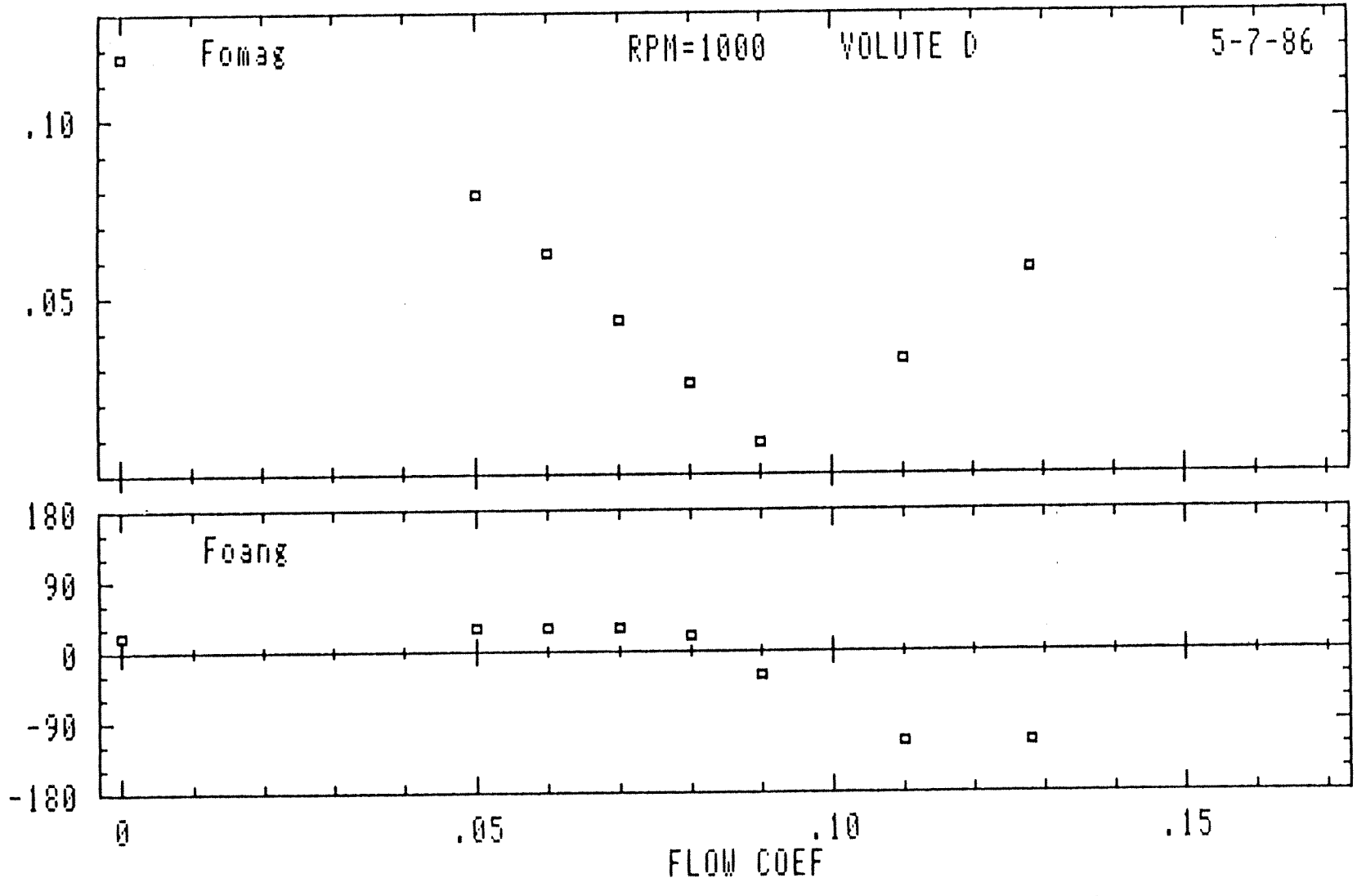
Fomag
RPM=1000
VOLUTE D
5-7-86
.10
.05
180
90
0
-90
-180
Foang
0
.05
.10
.15
FLOW COEF

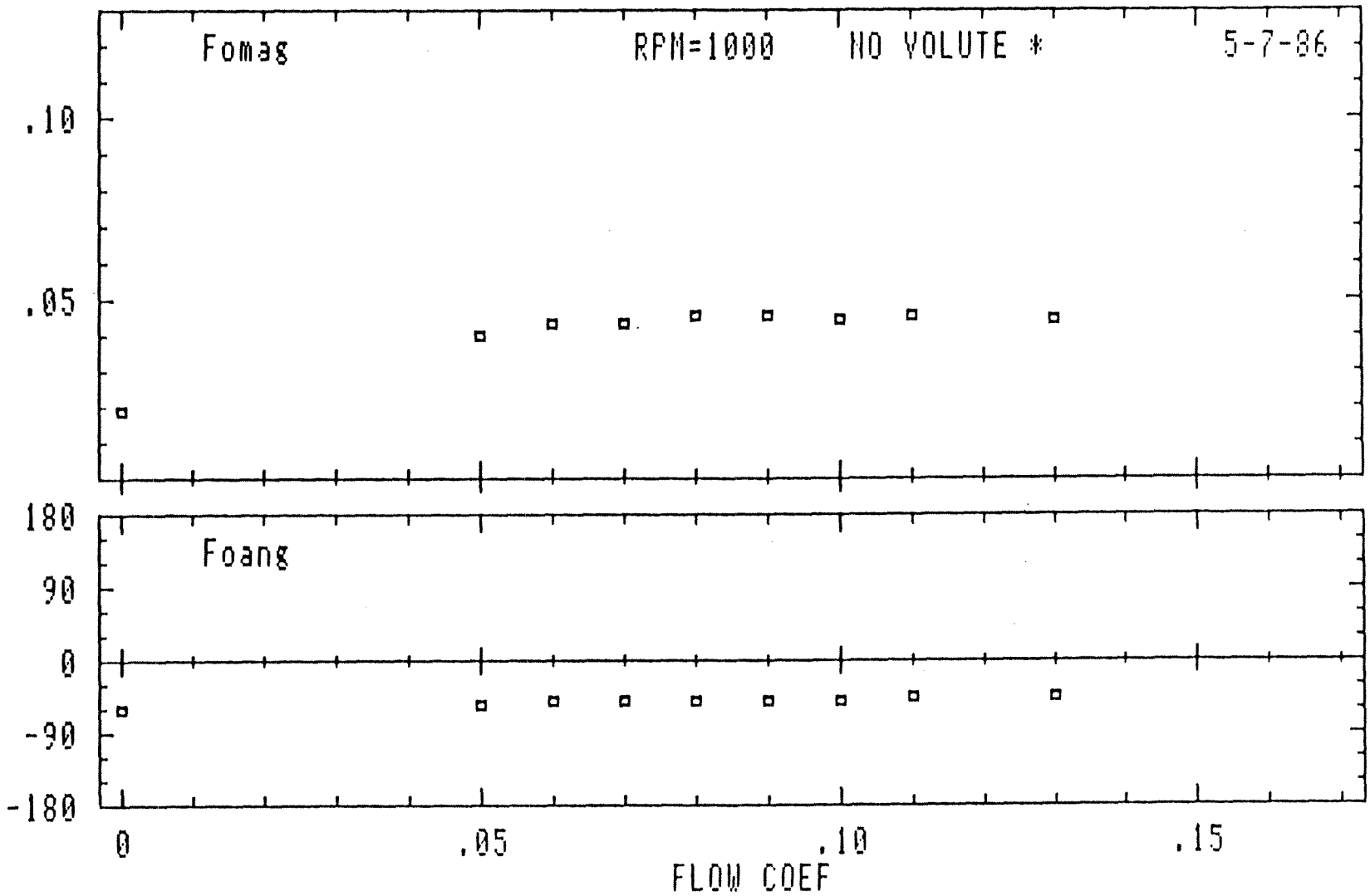
Fomag
RPM=1000
NO VOLUTE *
5-7-86
.10
.05
Foang
180
90
0
-90
-180
0
.05
.10
.15
FLOW COEF

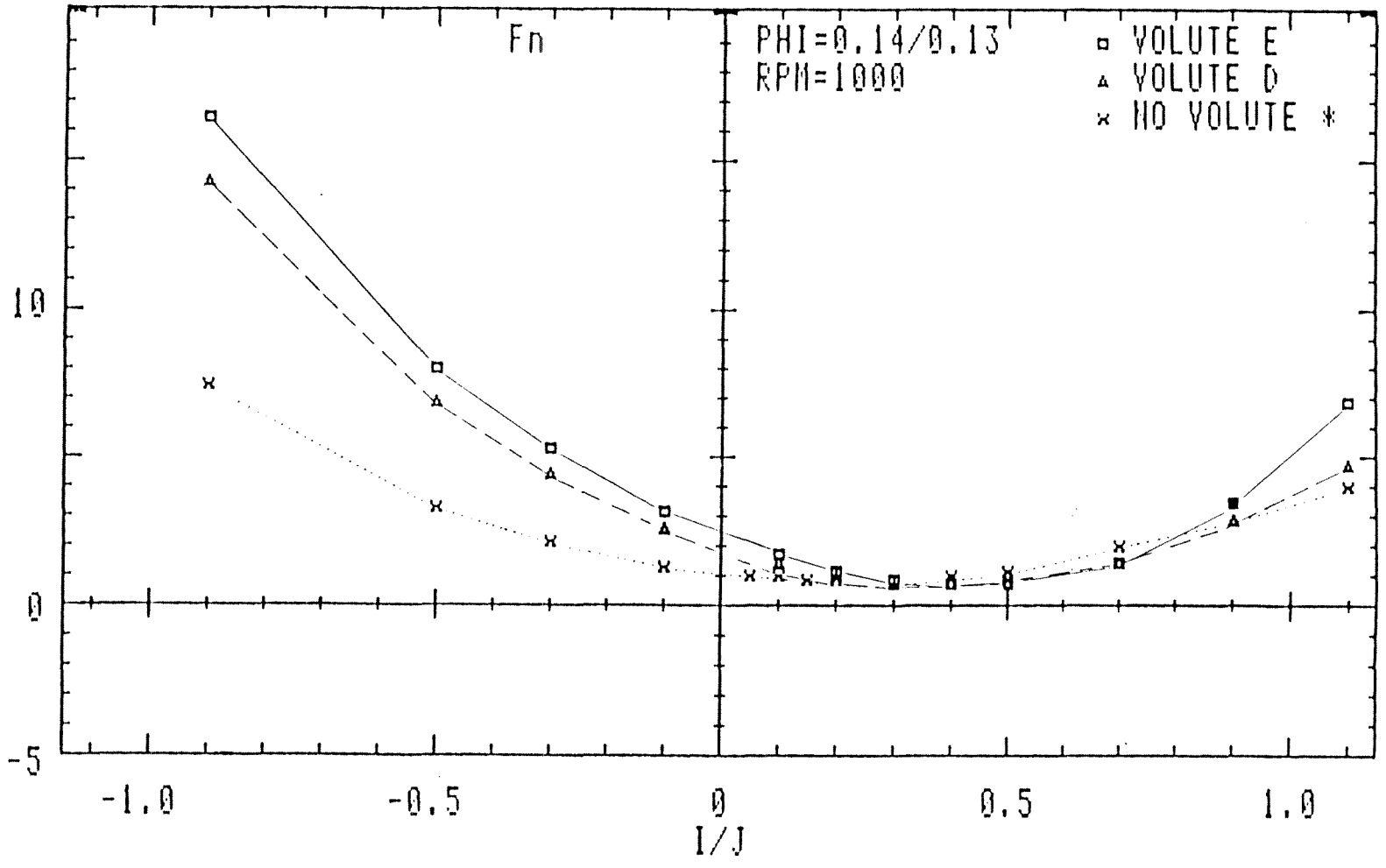
Fn
PHI=0.14/0.13
RPM=1000
VOLUTE E
VOLUTE D
NO VOLUTE *
10
0
-5
-1.0
-0.5
0
0.5
1.0
I/J

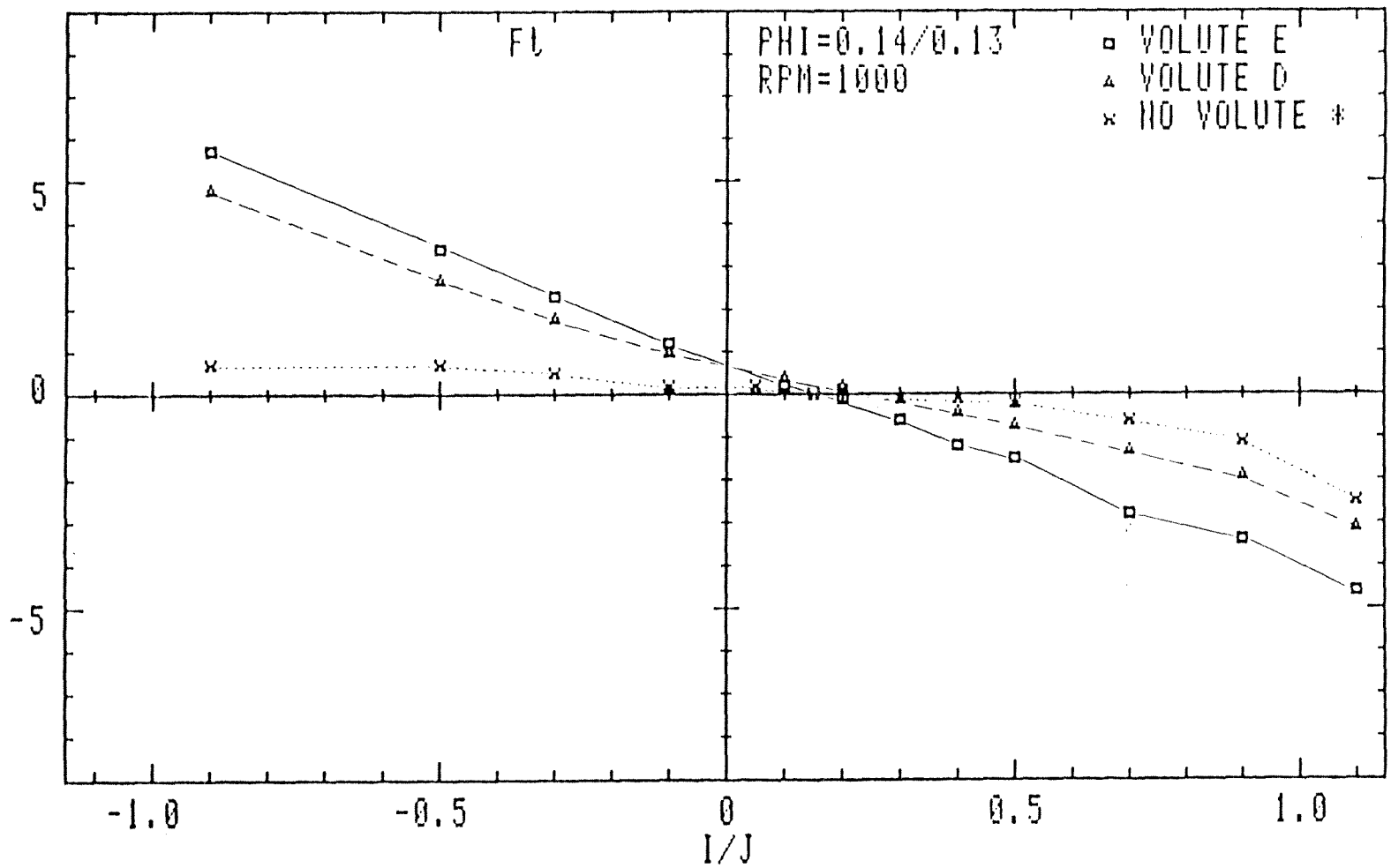
Fl
PHI=0.14/0.13
RPM=1000
VOLUTE E
VOLUTE D
NO VOLUTE *
5
0
-5
-1.0
-0.5
0
0.5
1.0
I/J

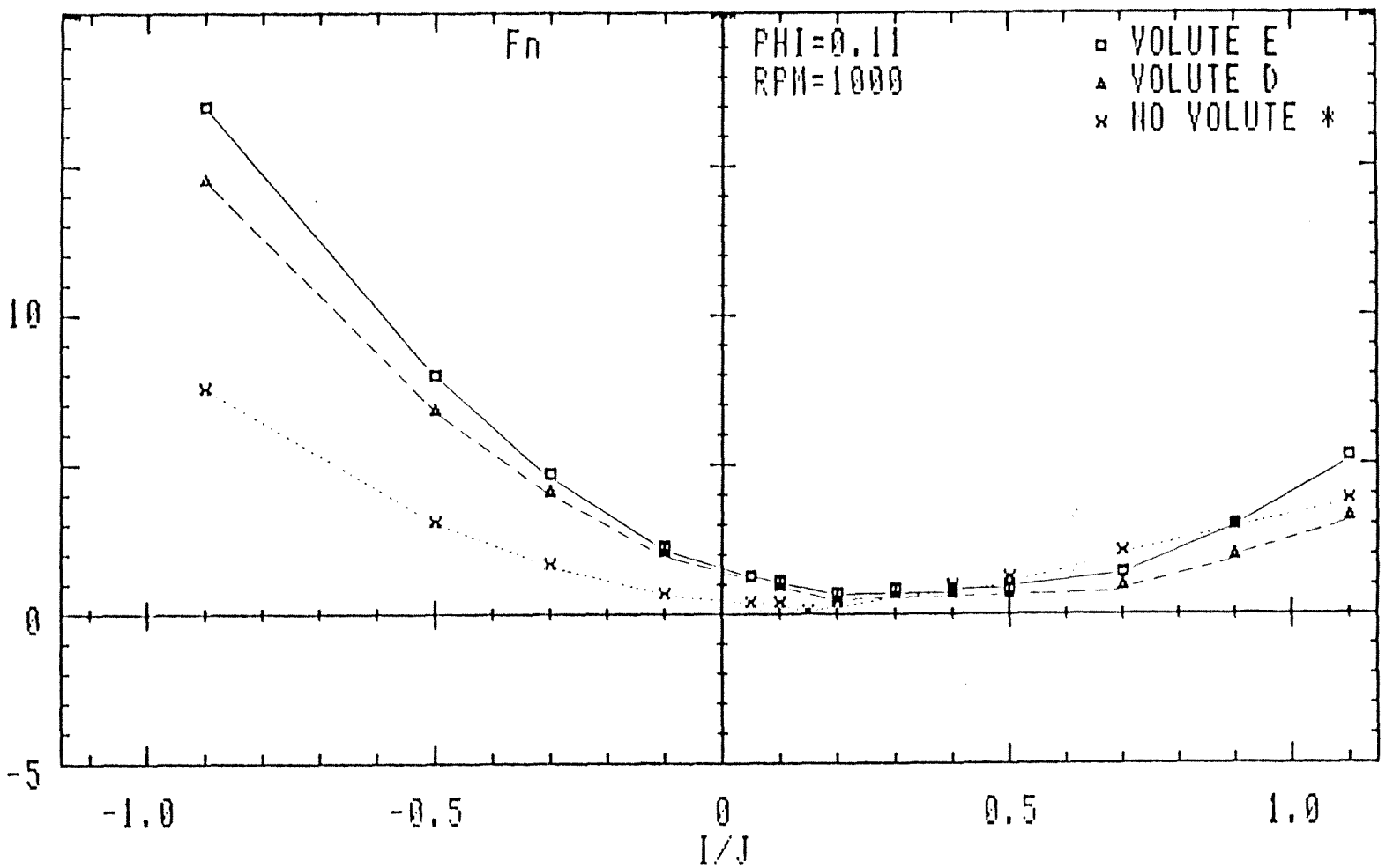
Fn
PHI=0.11
RPM=1000
VOLUTE E
VOLUTE D
NO VOLUTE *
10
0
-5
-1.0
-0.5
0
0.5
1.0
I/J

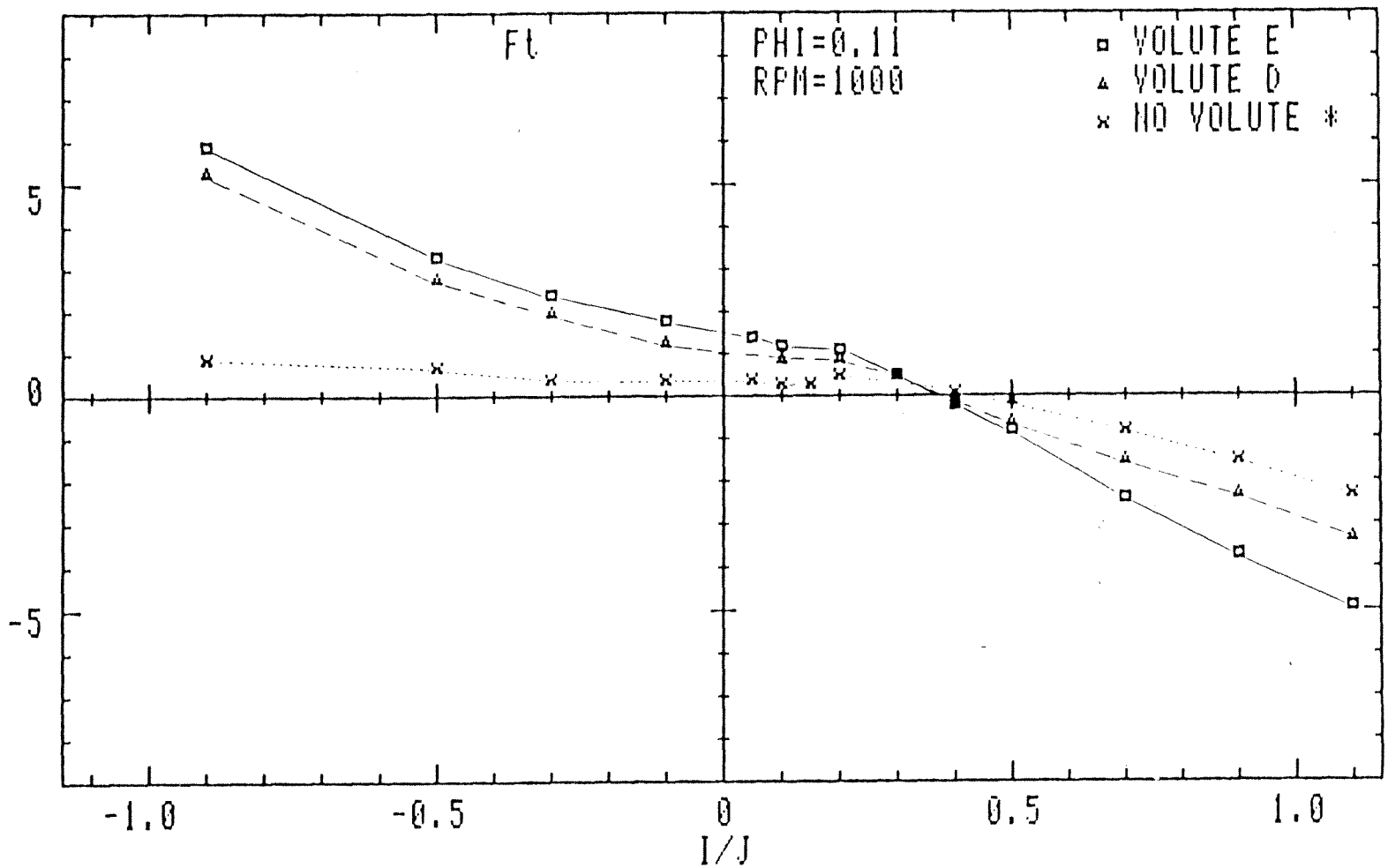
Fl
PHI=0.11
RPM=1000
VOLUTE E
VOLUTE D
NO VOLUTE *
5
0
-5
-1.0
-0.5
0
0.5
1.0
I/J

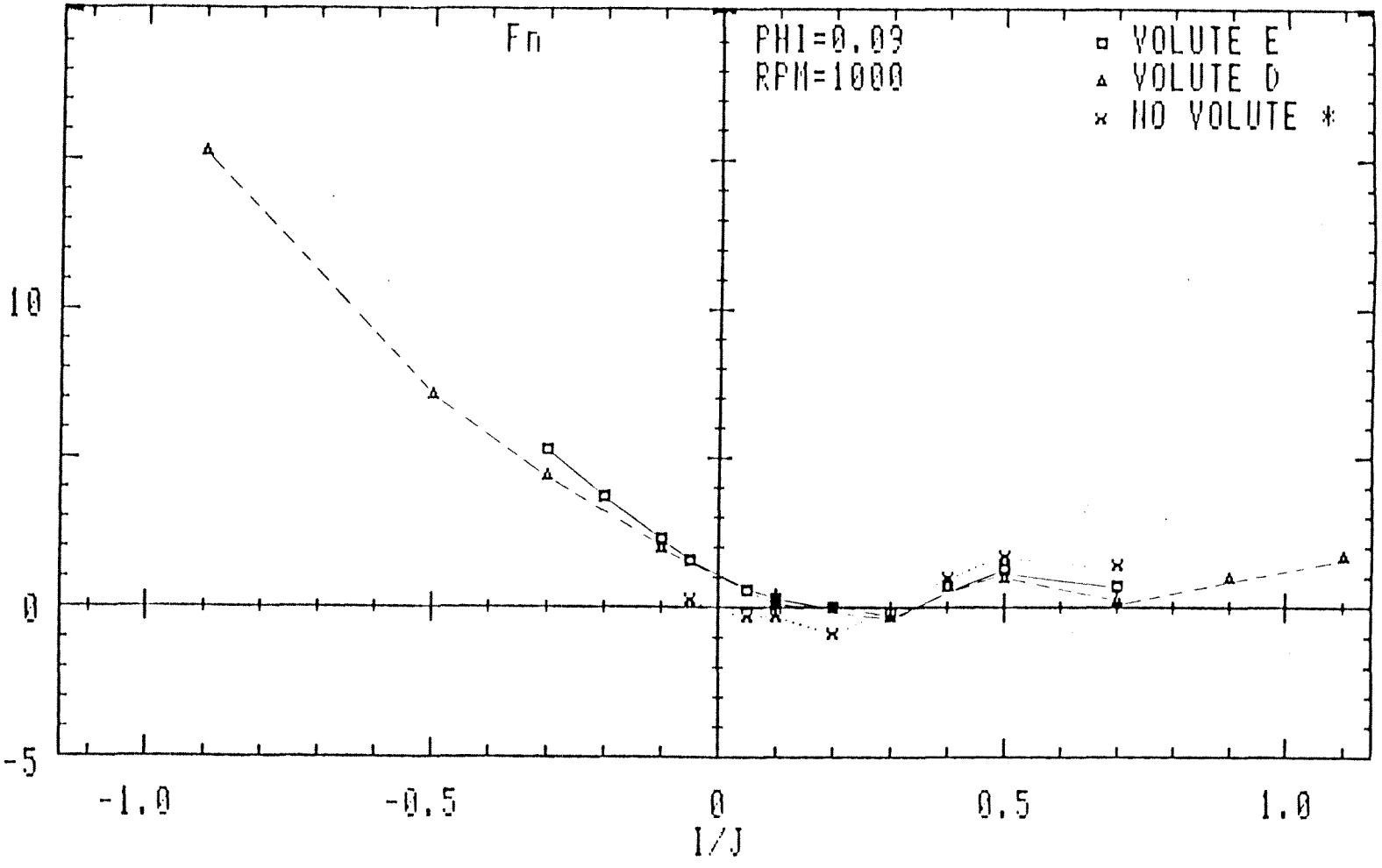
Fn
PHI=0.09
RPM=1000
VOLUTE E
VOLUTE D
NO VOLUTE *
10
0
-5
-1.0
-0.5
0
0.5
1.0
I/J

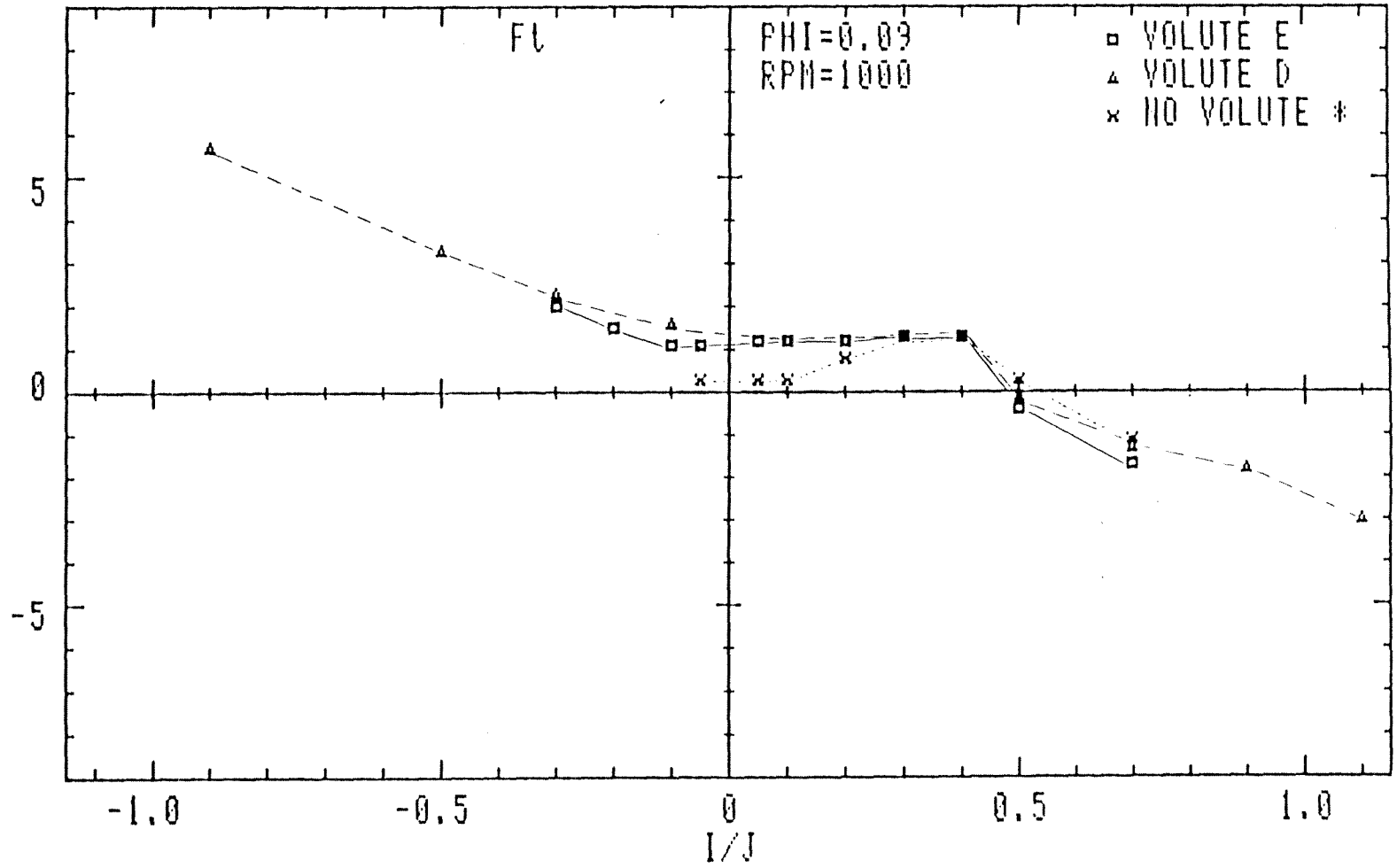
FL
PHI=0.09
RPM=1000
VOLUTE E
VOLUTE D
NO VOLUTE *
5
0
-5
-1.0
-0.5
0
0.5
1.0
I/J

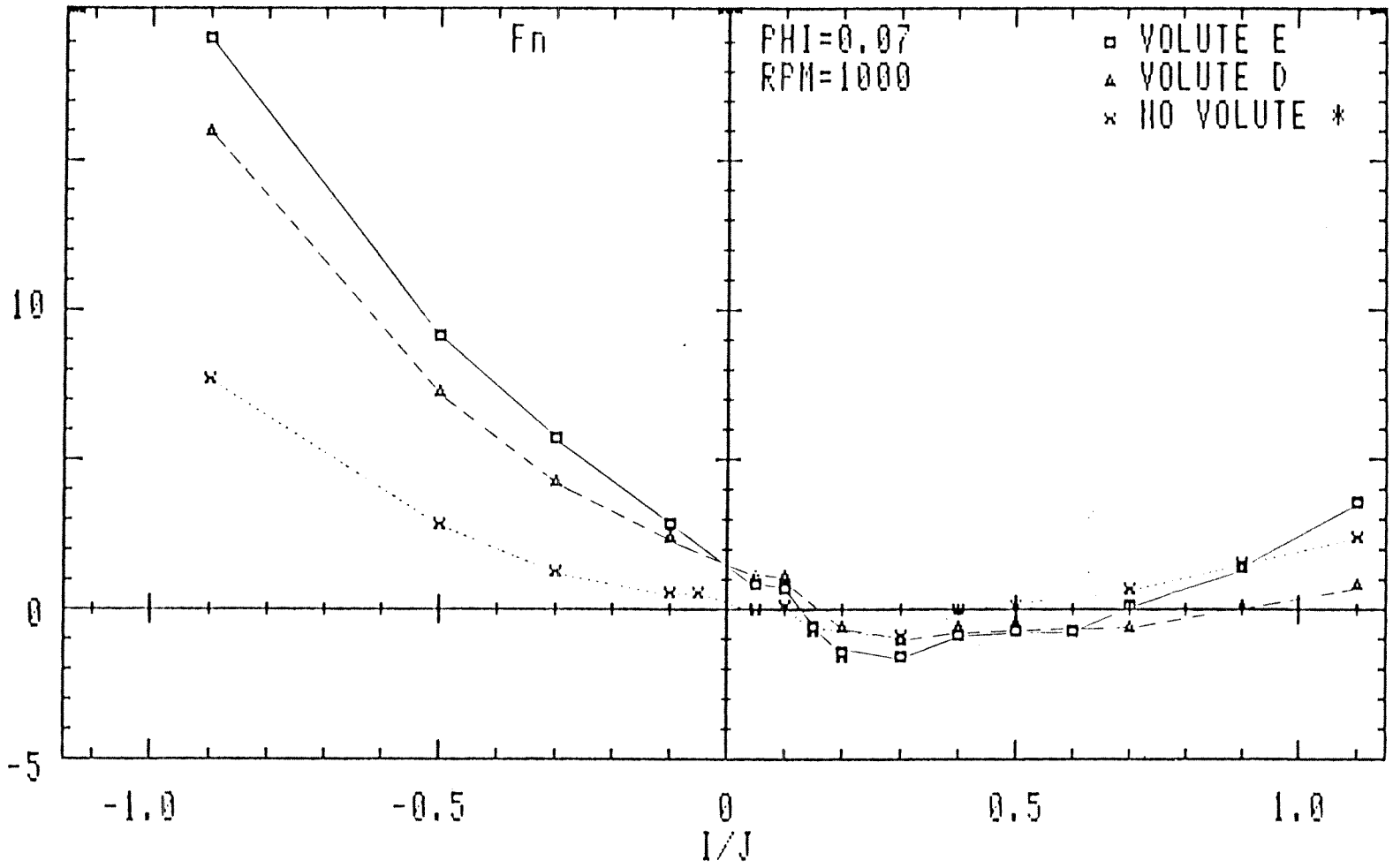
Fn
PHI=0.07
RPM=1000
VOLUTE E
VOLUTE D
NO VOLUTE *
10
0
-5
-1.0
-0.5
0
0.5
1.0
I/J

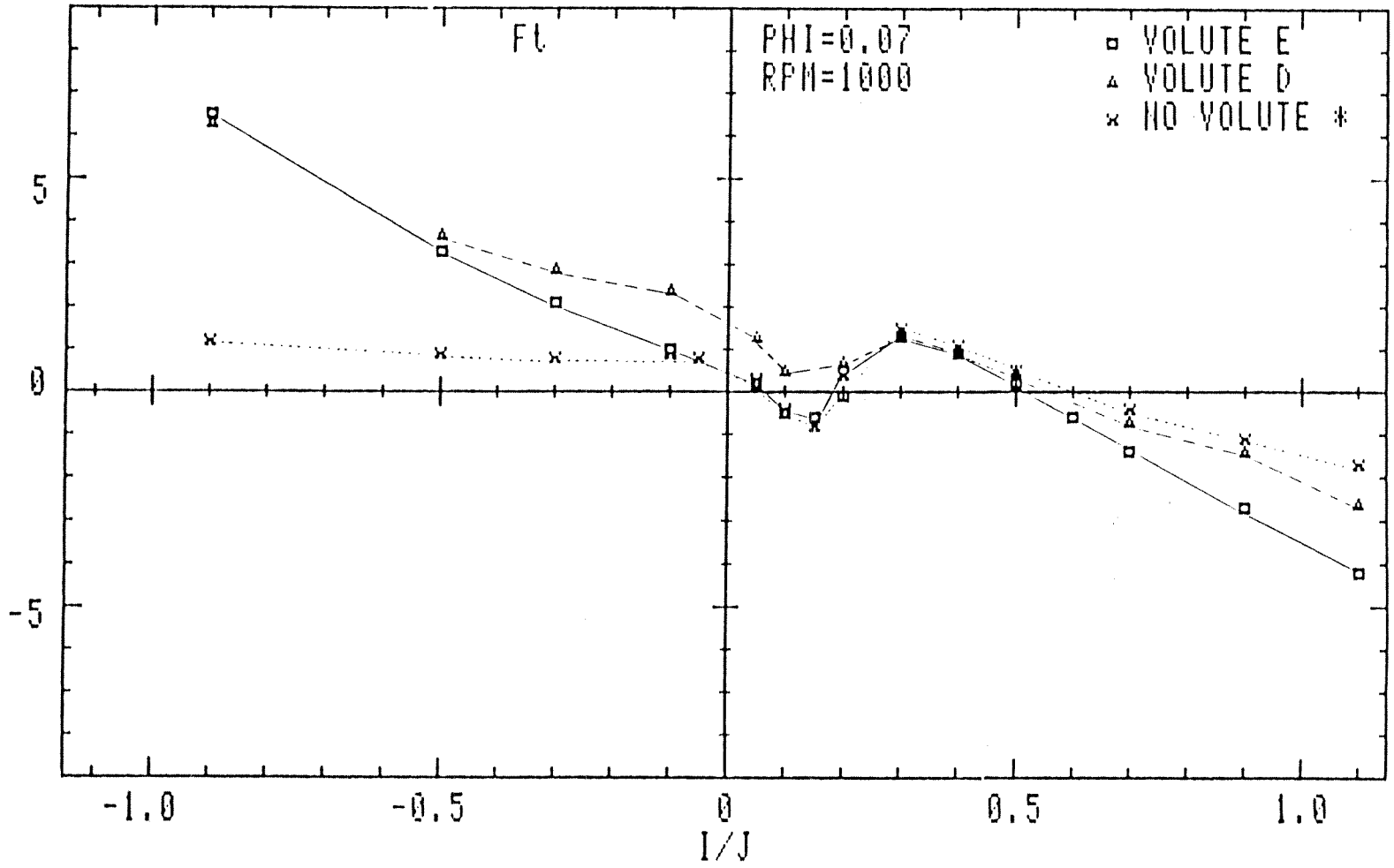
Ft
PHI=0.07
RPM=1000
VOLUTE E
VOLUTE D
NO VOLUTE *
5
0
-5
-1.0
-0.5
0
0.5
1.0
I/J

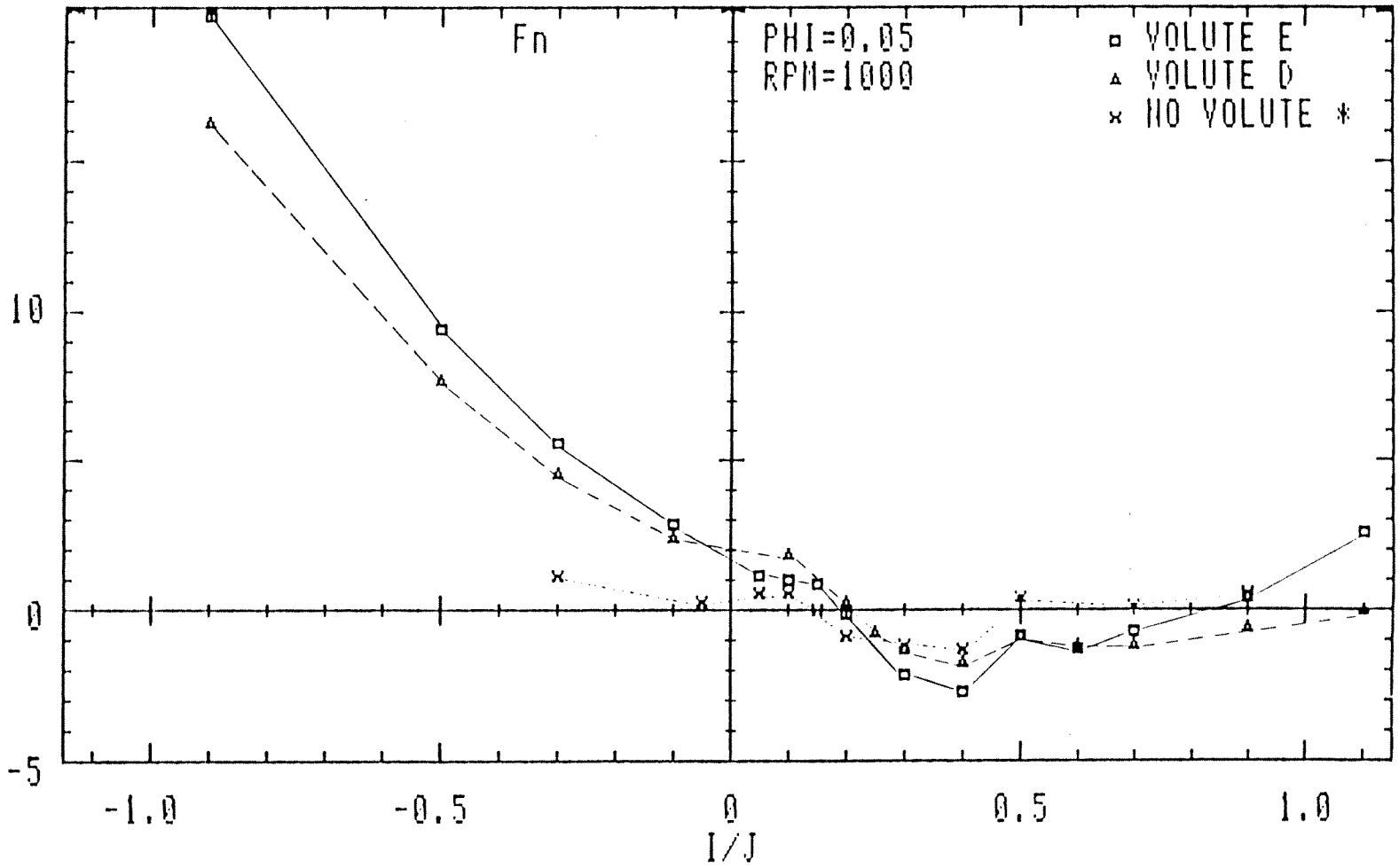
Fn
PHI=0.05
RPM=1000
VOLUTE E
VOLUTE D
NO VOLUTE *
10
0
-5
-1.0
-0.5
0
0.5
1.0
I/J

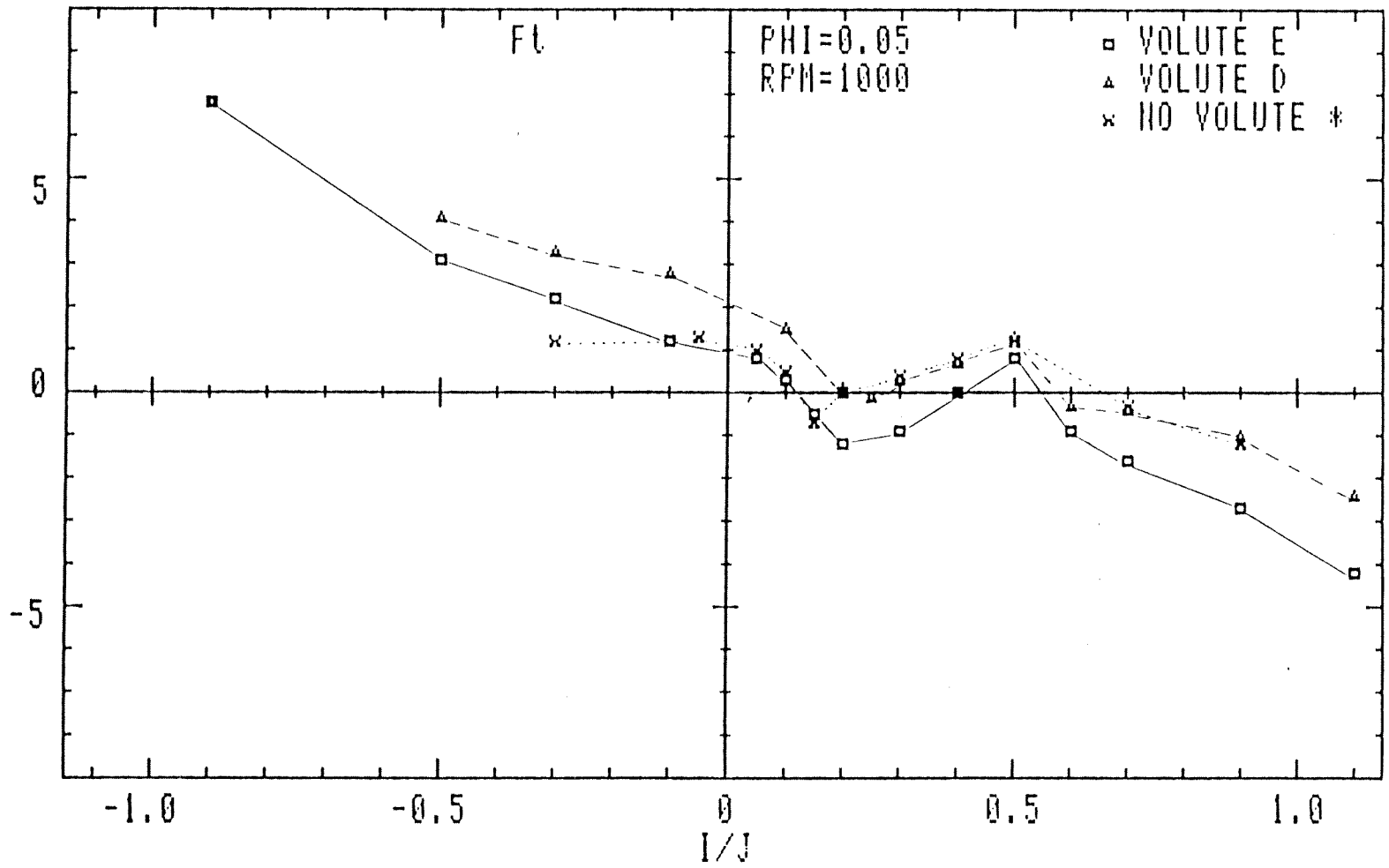
Ft
PHI=0.05
RPM=1000
VOLUTE E
VOLUTE D
NO VOLUTE *
5
0
-5
-1.0
-0.5
0
0.5
1.0
I/J

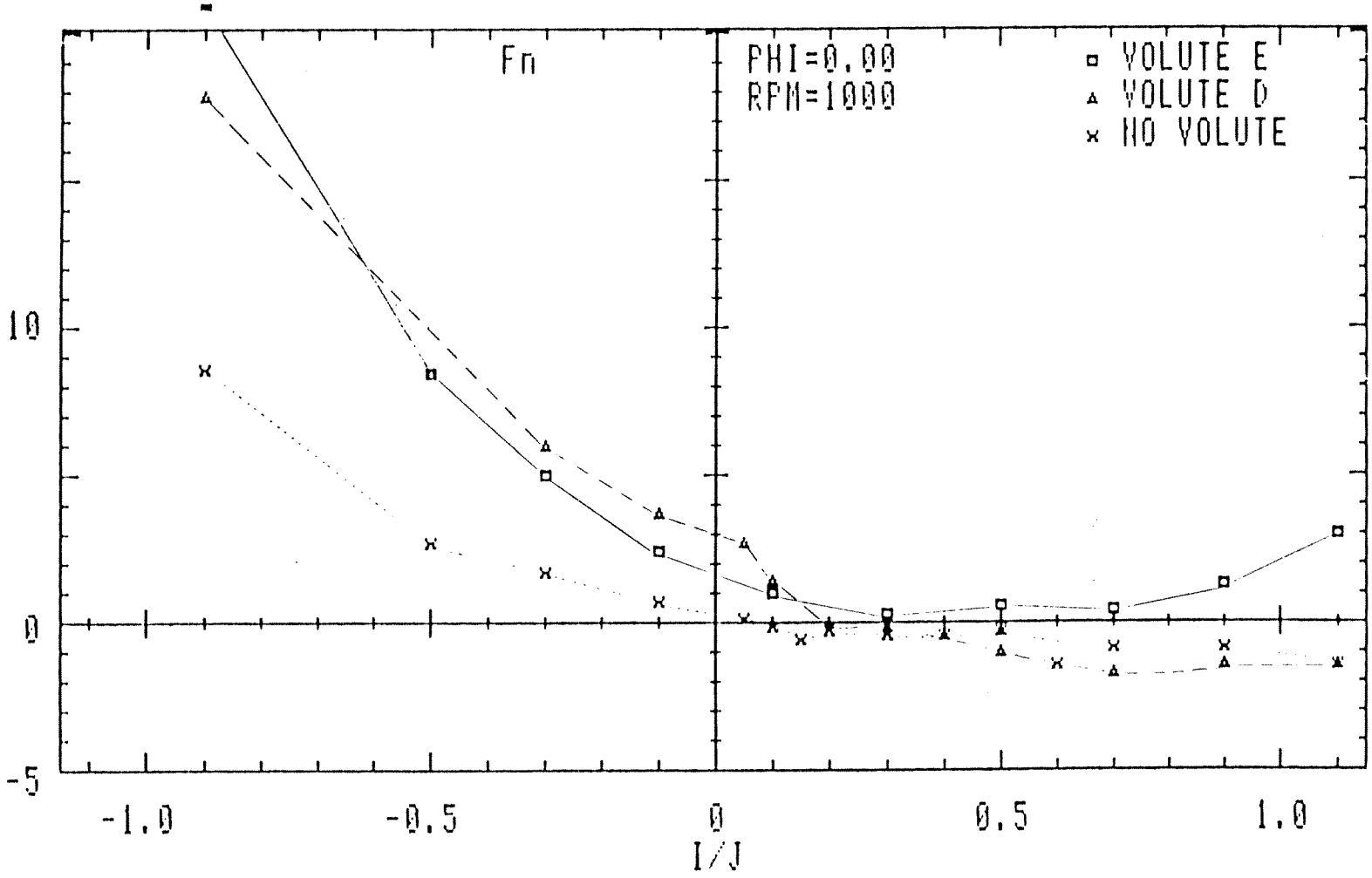
Fn
PHI=0.00
RPM=1000
VOLUTE E
VOLUTE D
NO VOLUTE
10
0
-5
-1.0
-0.5
0
0.5
1.0
I/J

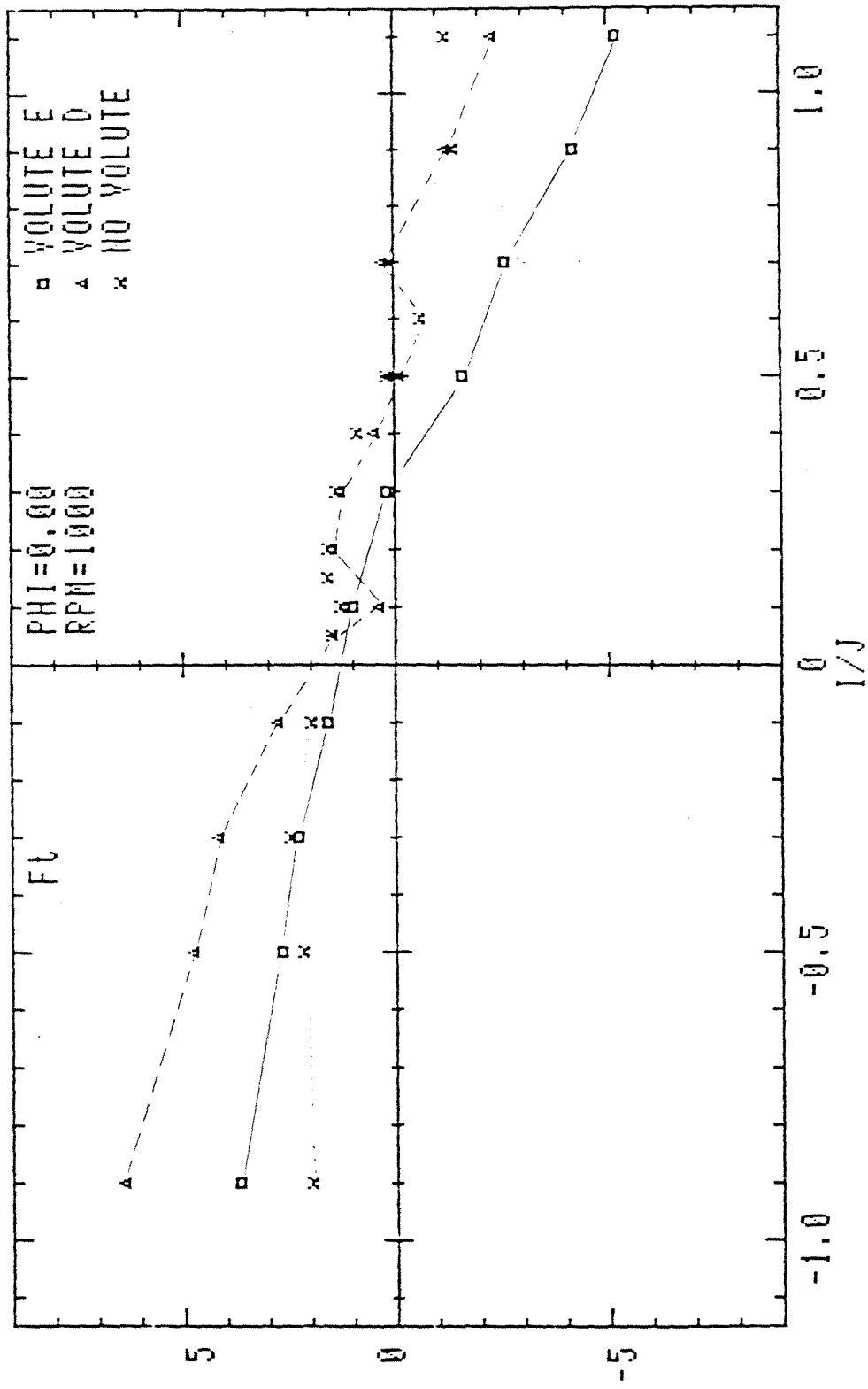
VOLUTE E
VOLUTE D
NO VOLUTE
PHI=0.00
RPM=1000
Ft
5
0
-5
-1.0
-0.5
0
0.5
1.0
I/J

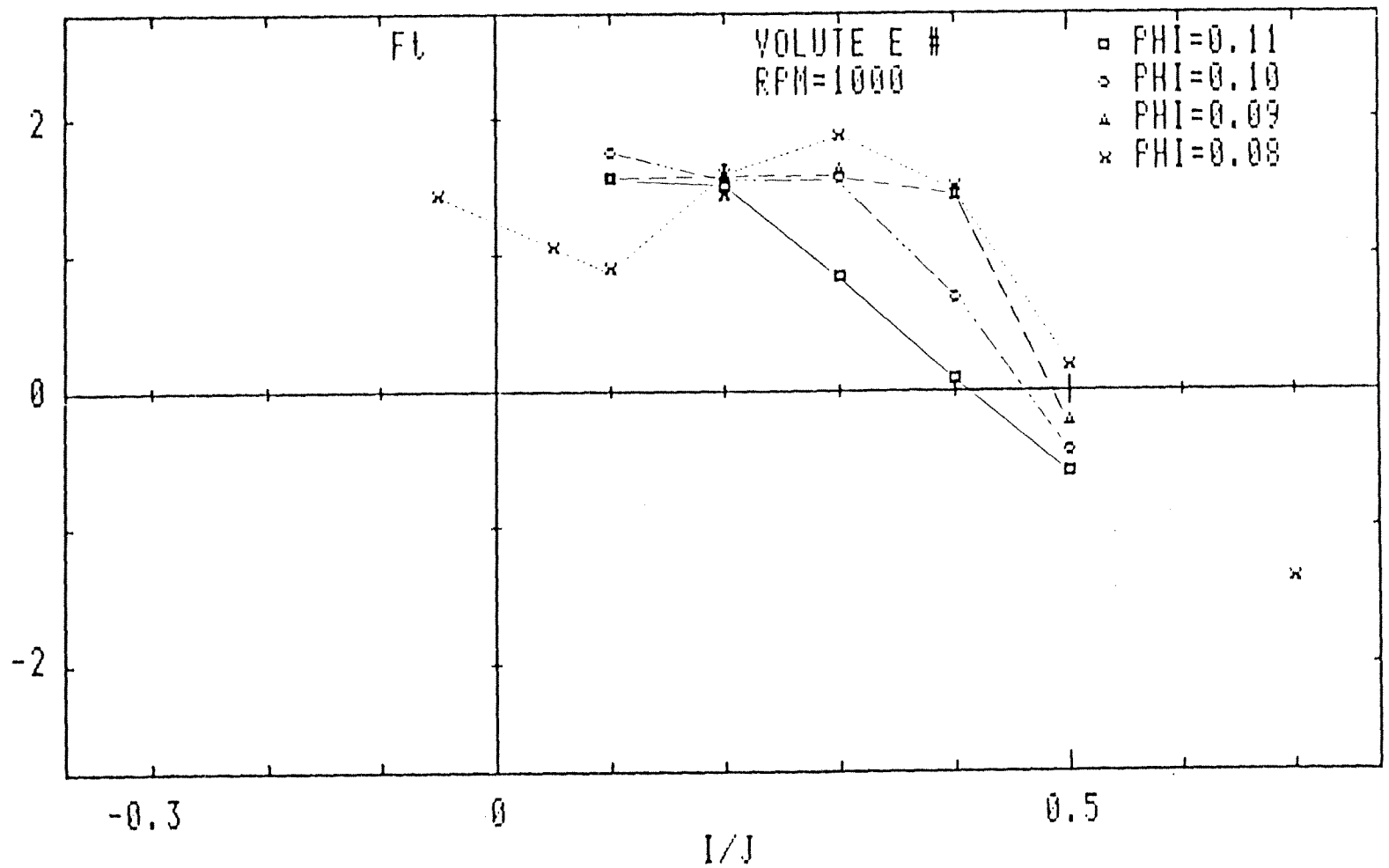
FL
VOLUTE E #
RPM=1000
PHI=0.11
PHI=0.10
PHI=0.09
PHI=0.08
2
0
-2
-0.3
0
0.5
I/J

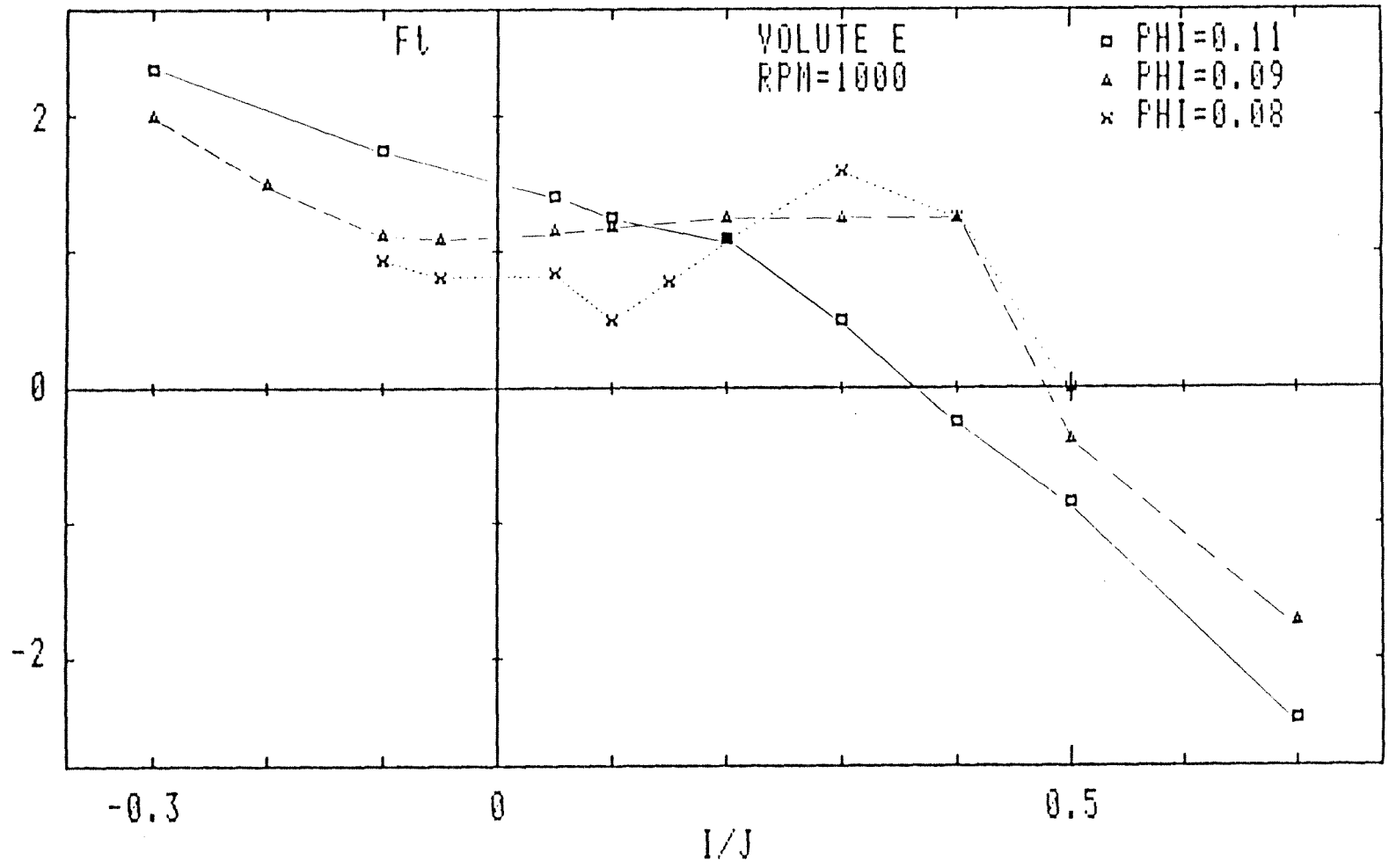
FL
VOLUTE E
RPM=1000
PHI=0.11
PHI=0.09
PHI=0.08
2
0
-2
-0.3
0
0.5
I/J

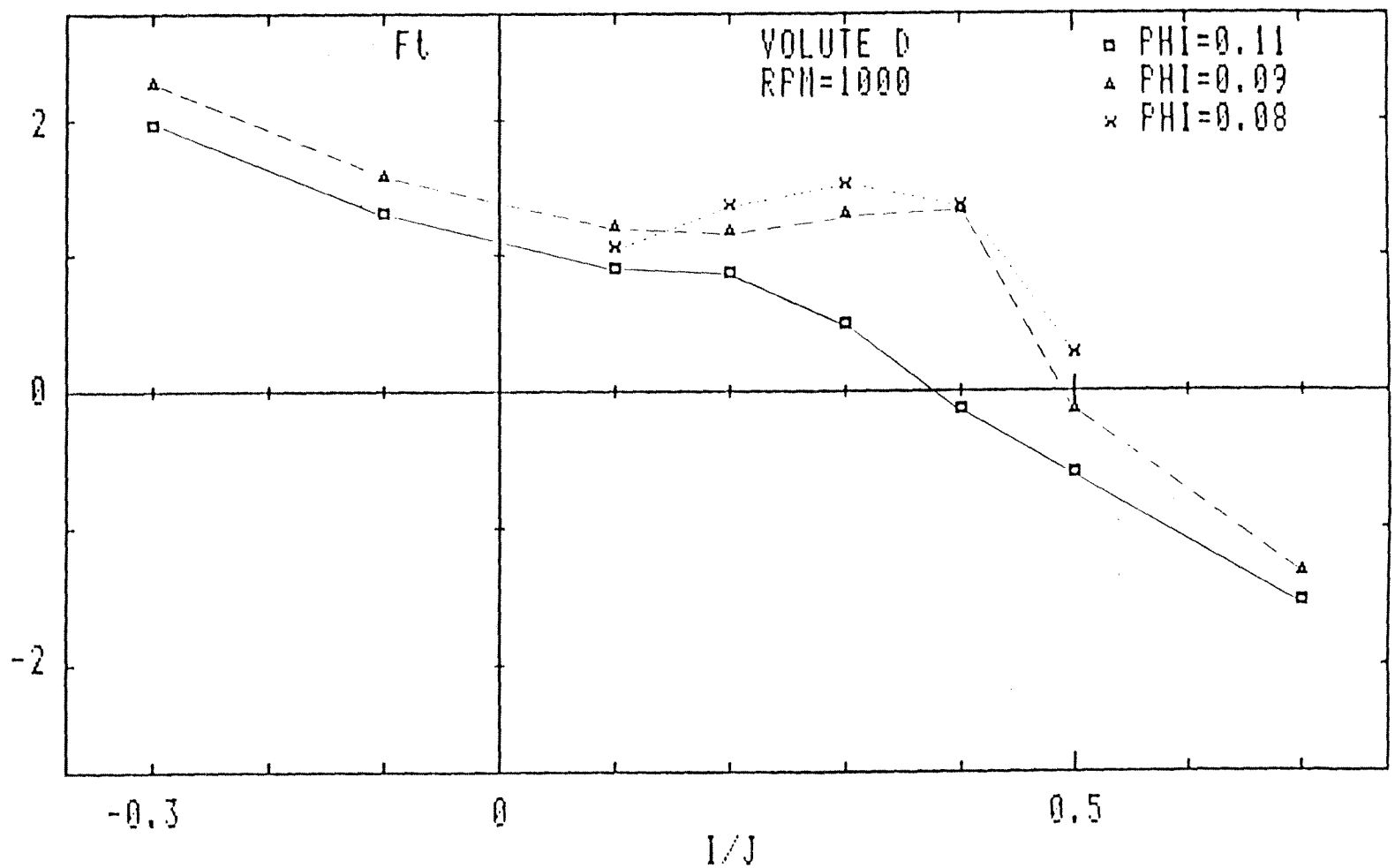
Ft
VOLUTE D
RPM=1000
PHI=0.11
PHI=0.09
PHI=0.08
2
0
-2
-0.3
0
0.5
I/J

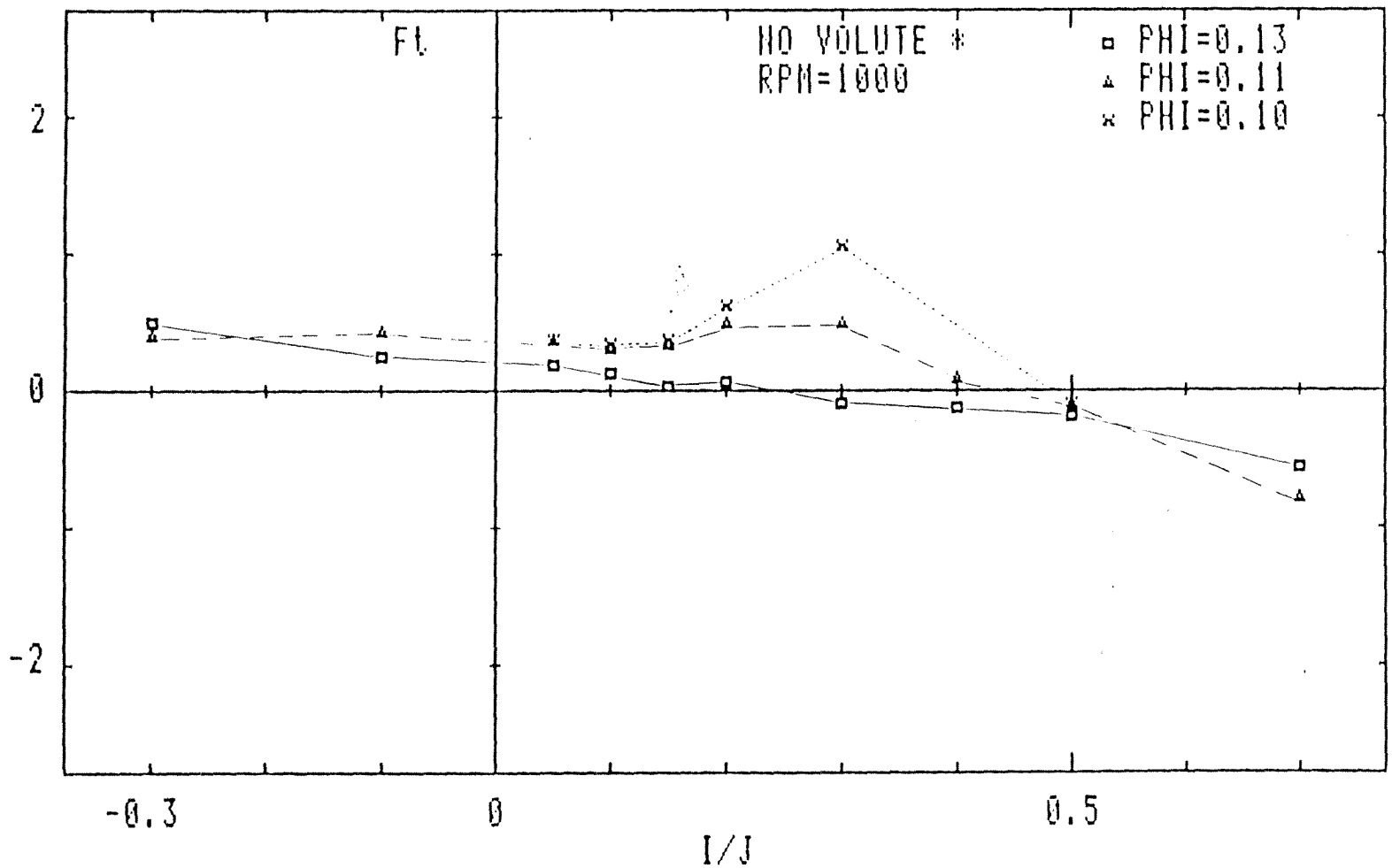
FL
NO VOLUTE *
RPM=1000
PHI=0.13
PHI=0.11
PHI=0.10
2
0
-2
-0.3
0
0.5
I/J

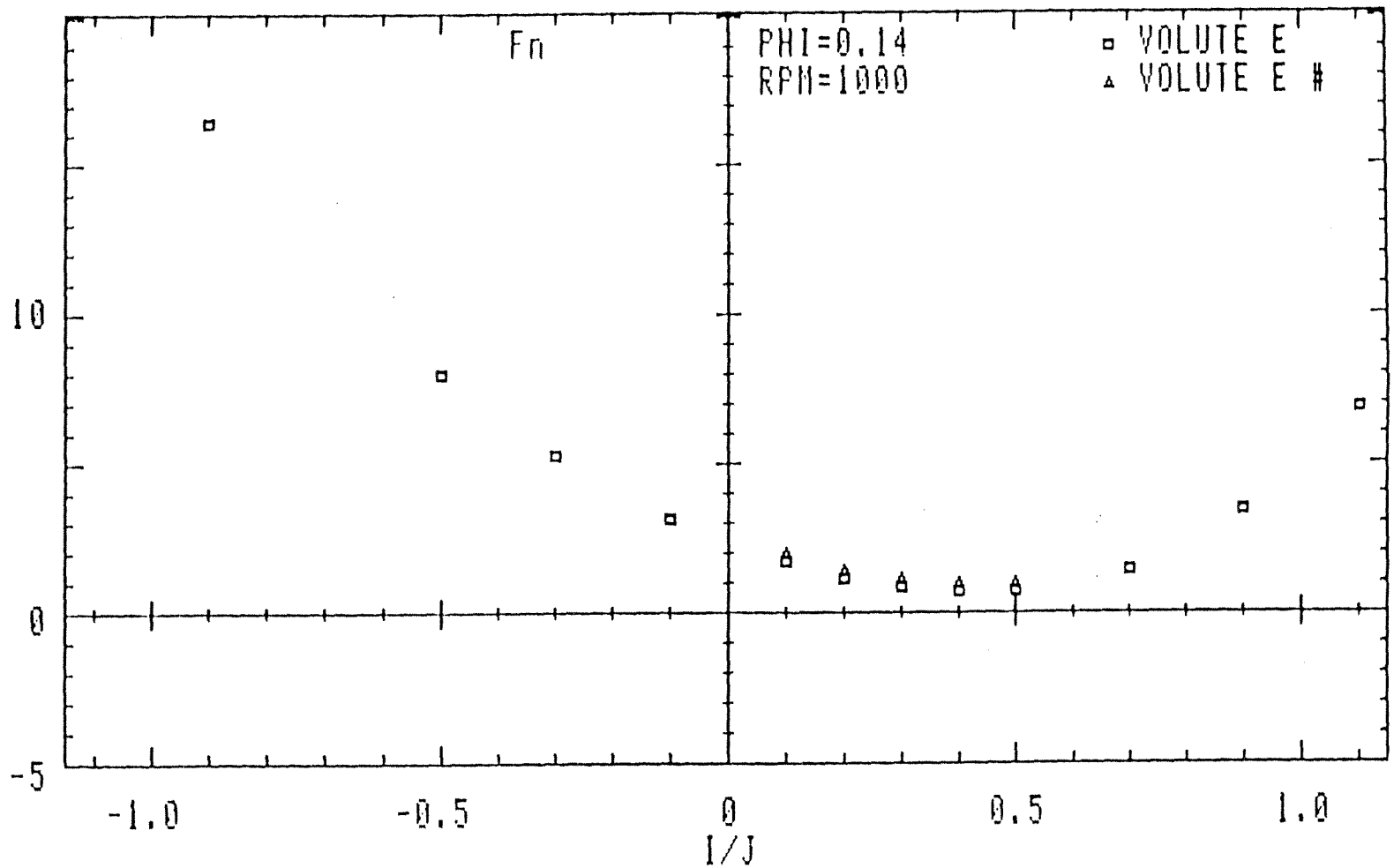
Fn
PHI=0.14
RPM=1000
VOLUTE E
VOLUTE E #
10
0
-5
-1.0
-0.5
0
0.5
1.0
I/J

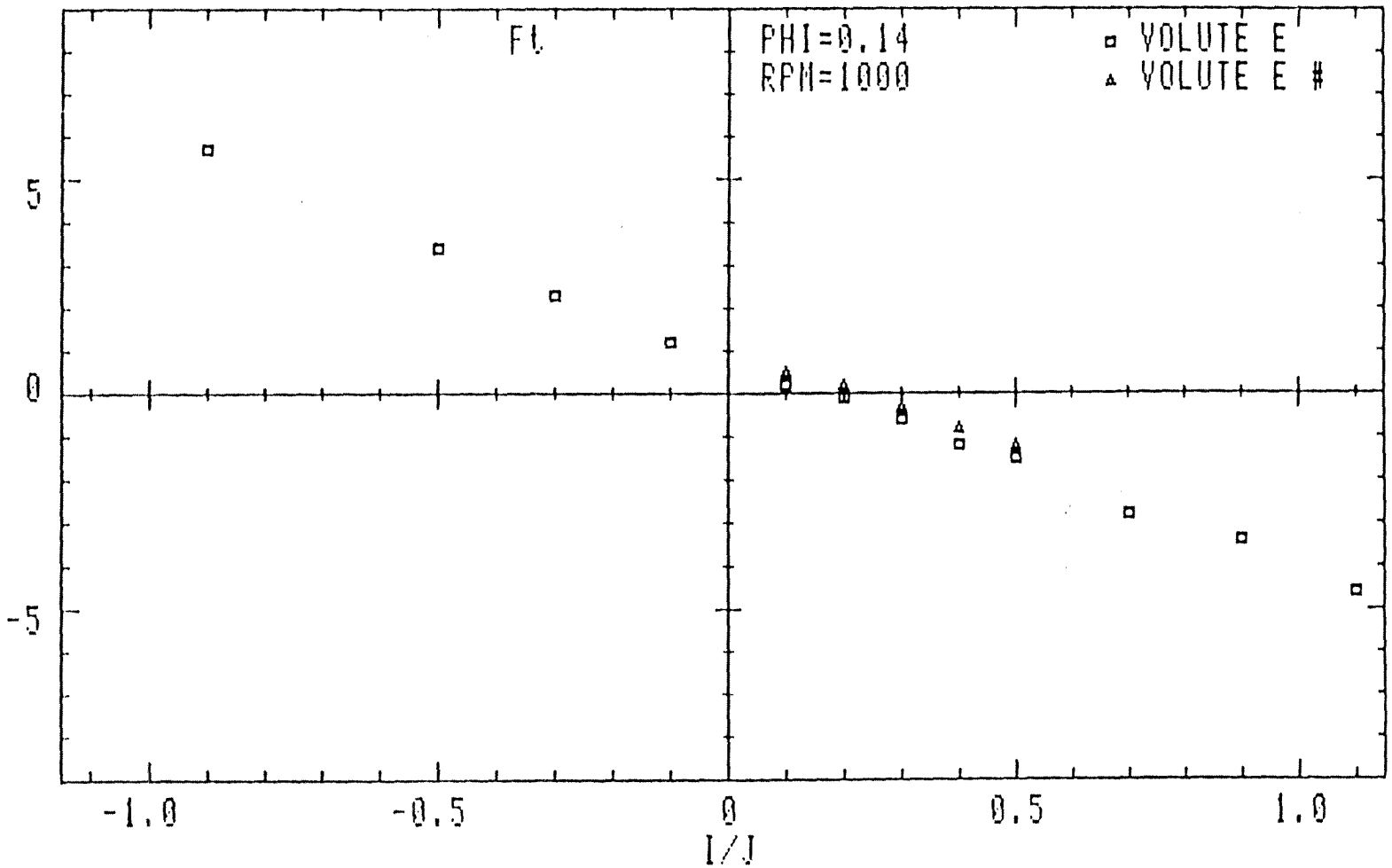
FL
PHI=0.14
RPM=1000
VOLUTE E
VOLUTE E #
5
0
-5
-1.0
-0.5
0
0.5
1.0
I/J

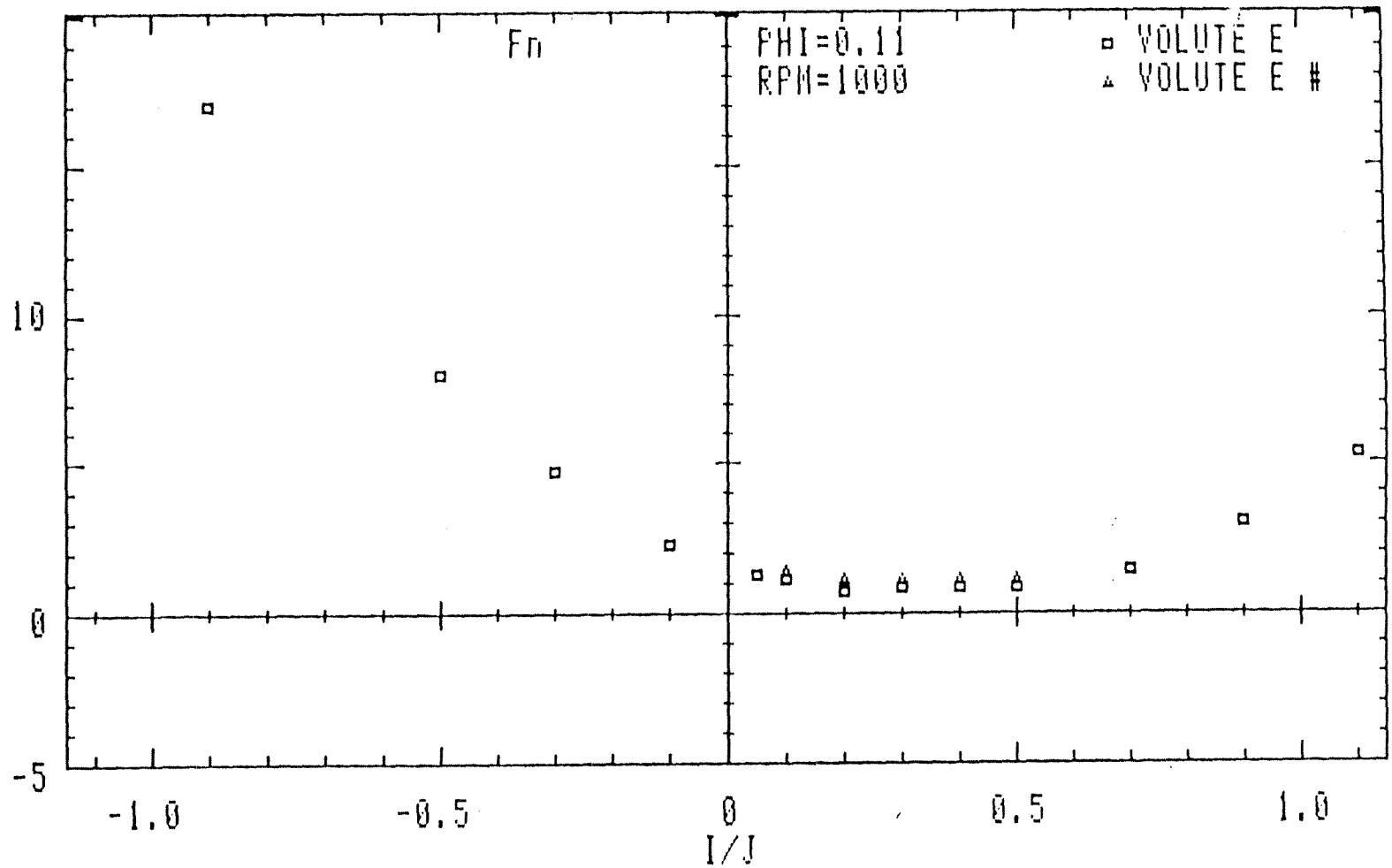
Fn
PHI=0.11
RPM=1000
VOLUTE E
VOLUTE E #
10
0
-5
-1.0
-0.5
0
0.5
1.0
I/J

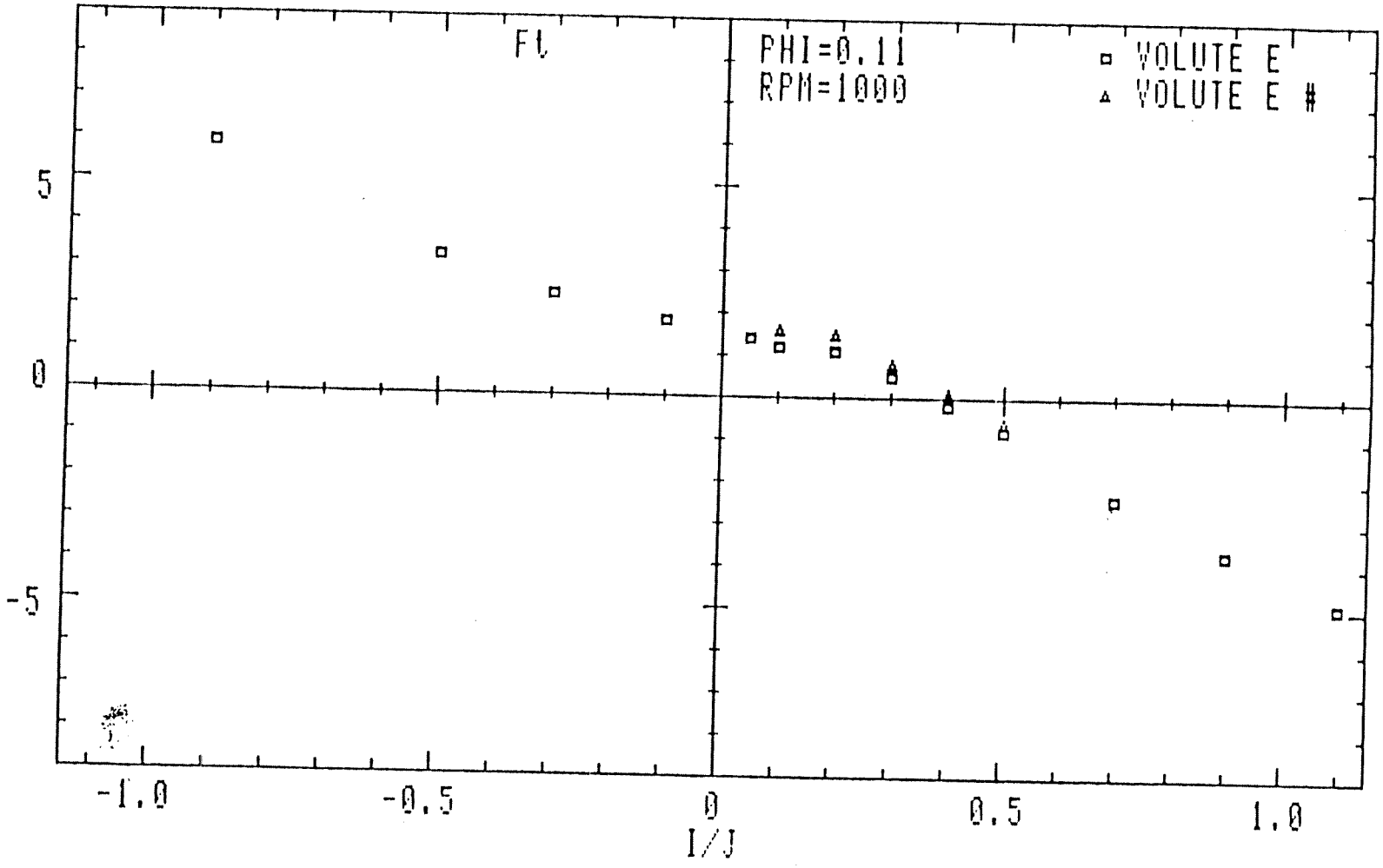
Ft
PHI=0.11
RPM=1000
VOLUTE E
VOLUTE E #
5
0
-5
-1.0
-0.5
0
0.5
1.0
I/J

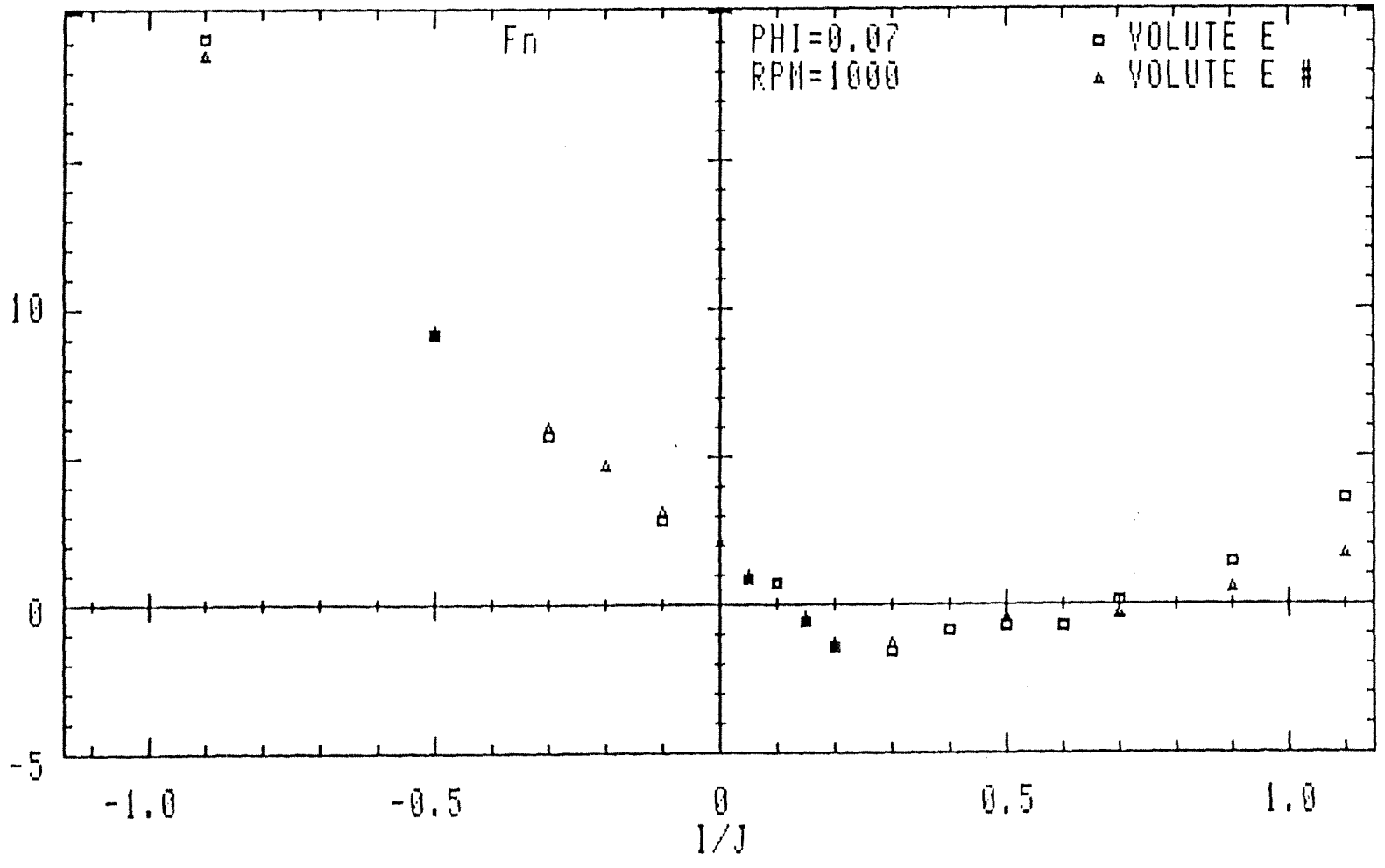
Fn
PHI=0.07
RPM=1000
VOLUTE E
VOLUTE E #
10
0
-5
-1.0
-0.5
0
0.5
1.0
I/J

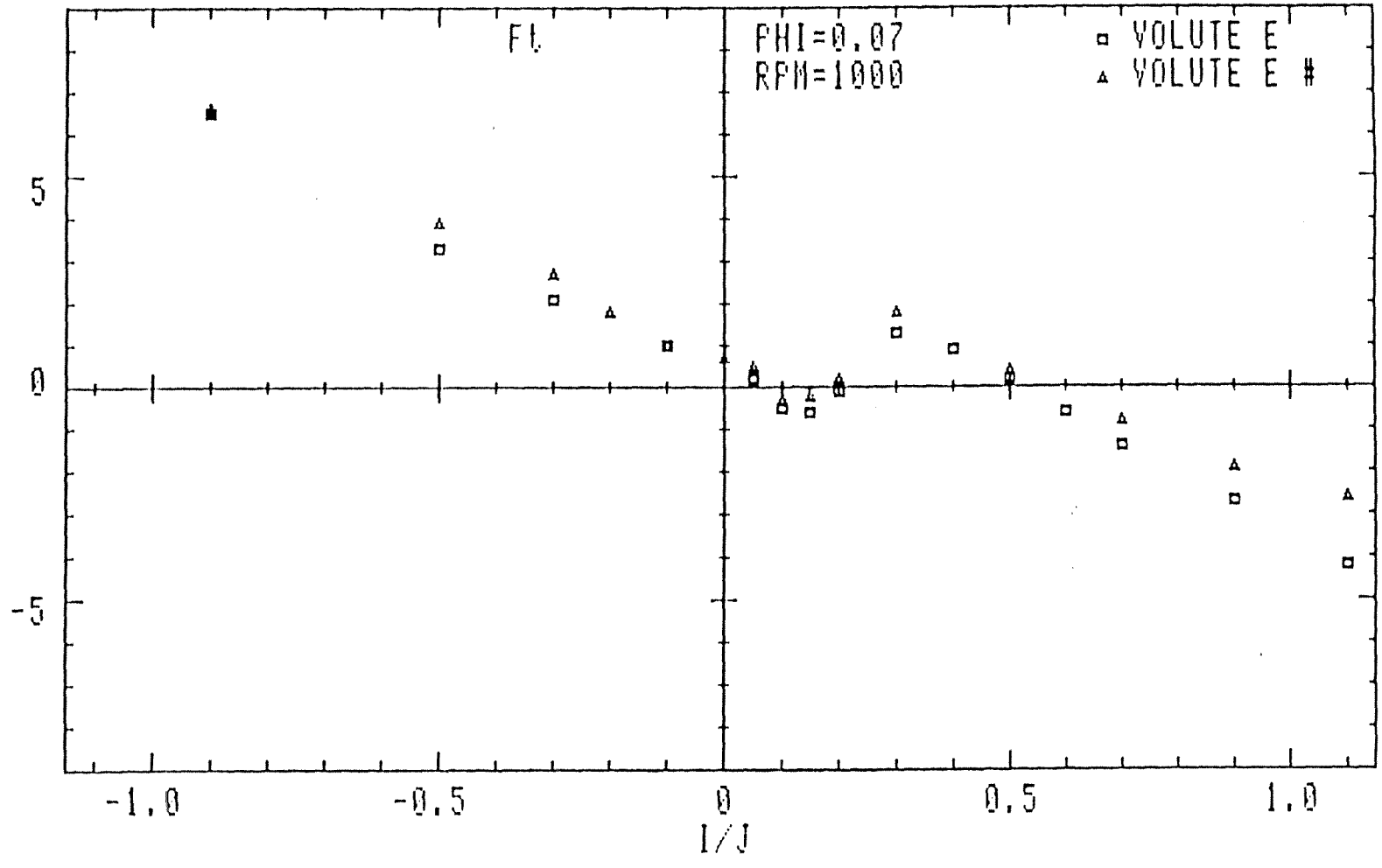
FL
PHI=0.07
RPM=1000
VOLUTE E
VOLUTE E #
5
0
-5
-1.0
-0.5
0
0.5
1.0
I/J

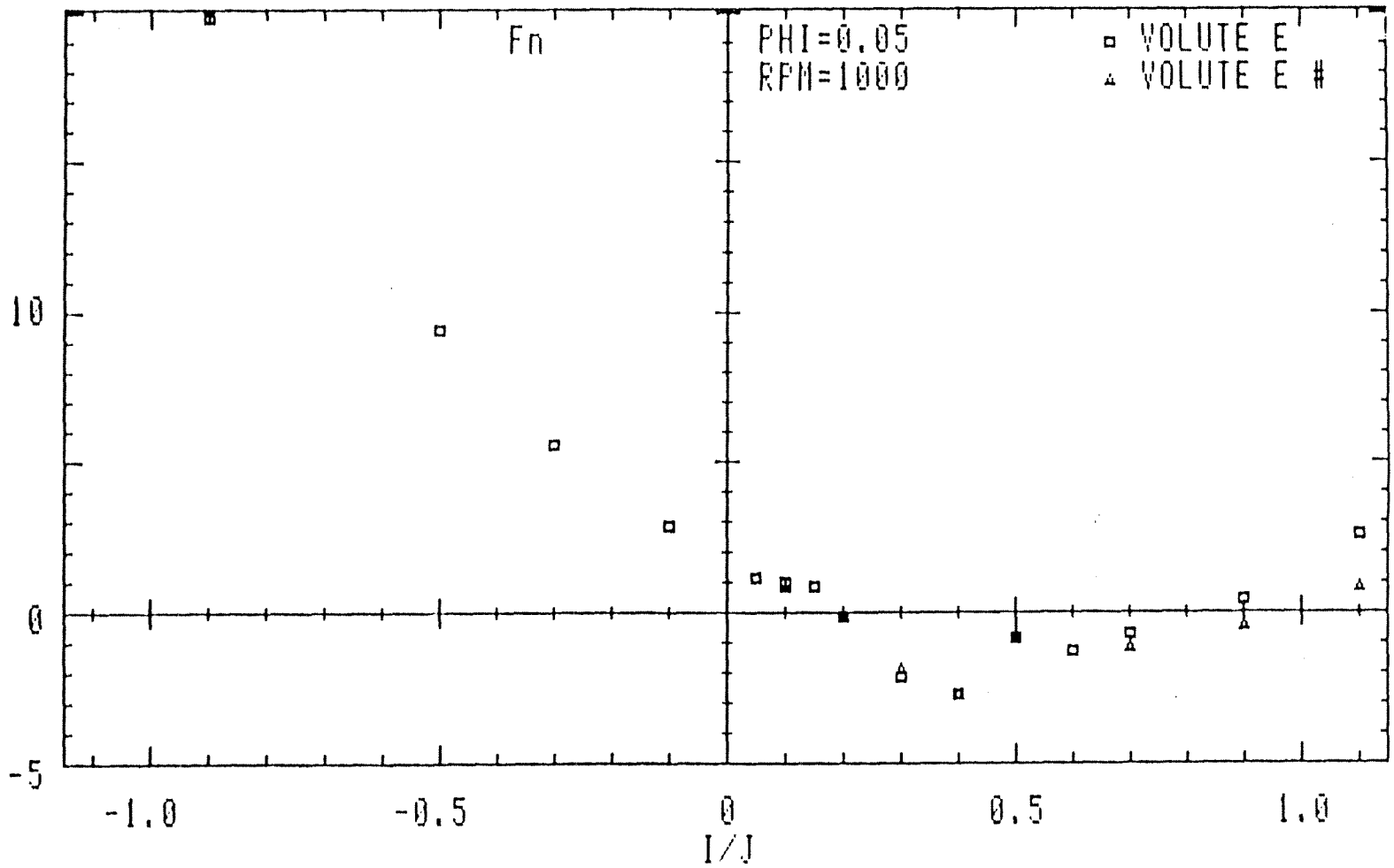
Fn
PHI=0.05
RPM=1000
VOLUTE E
VOLUTE E #
10
0
-5
-1.0
-0.5
0
0.5
1.0
I/J

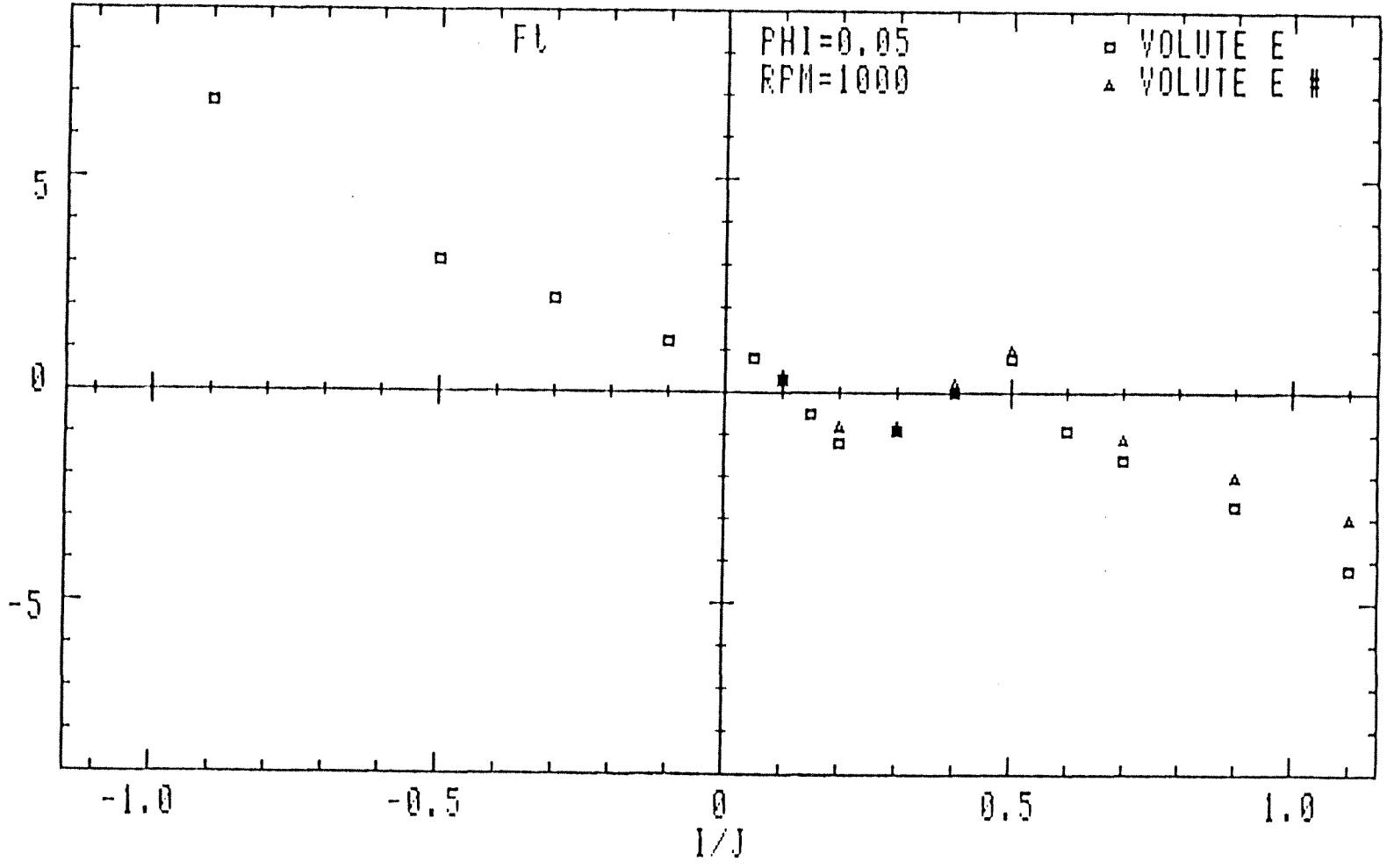
FL
PHI=0.05
RPM=1000
VOLUTE E
VOLUTE E #
5
0
-5
-1.0
-0.5
0
0.5
1.0
I/J

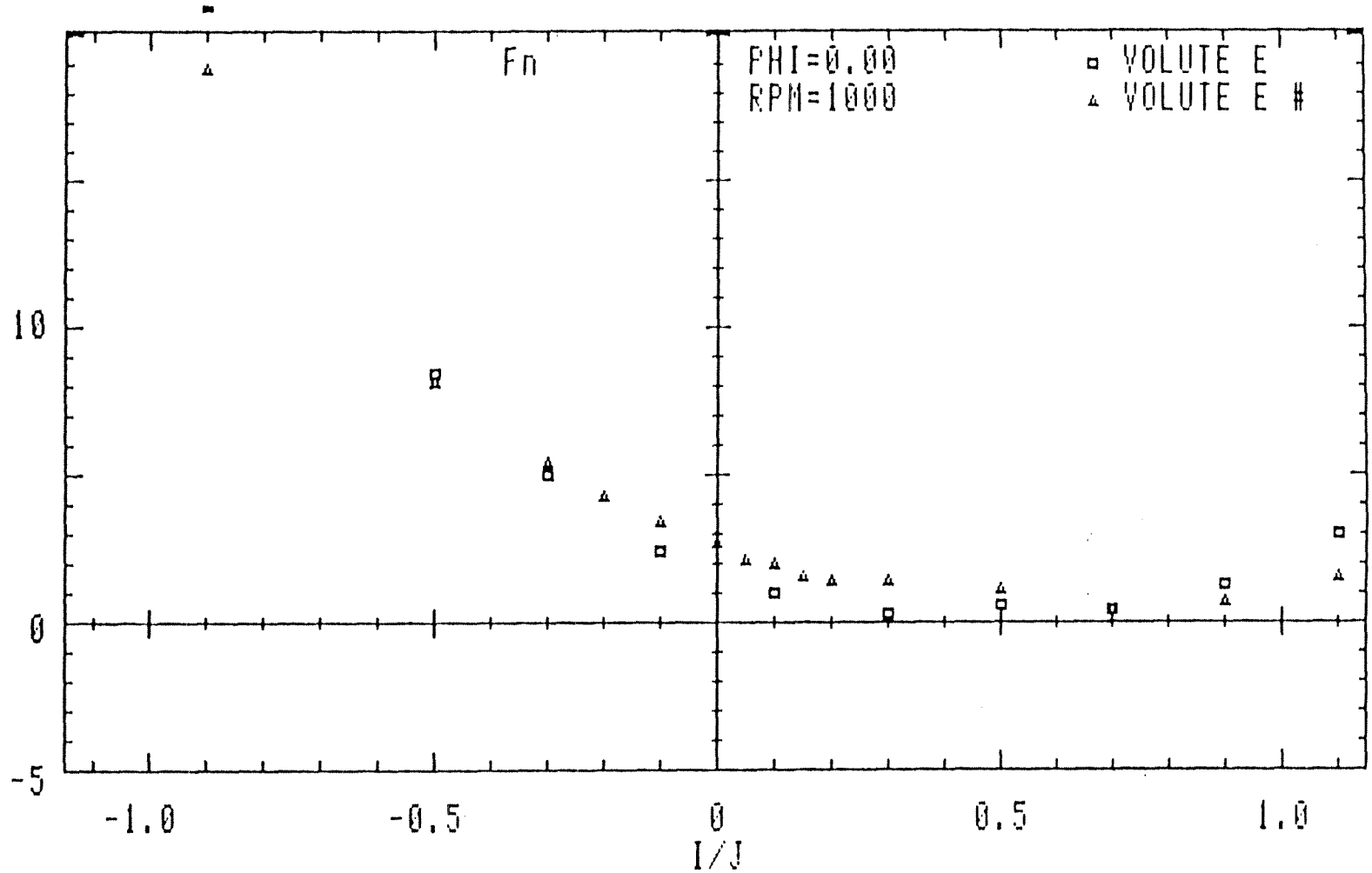
Fn
PHI=0.00
RPM=1000
VOLUTE E
VOLUTE E #
10
0
-5
-1.0
-0.5
0
0.5
1.0
I/J

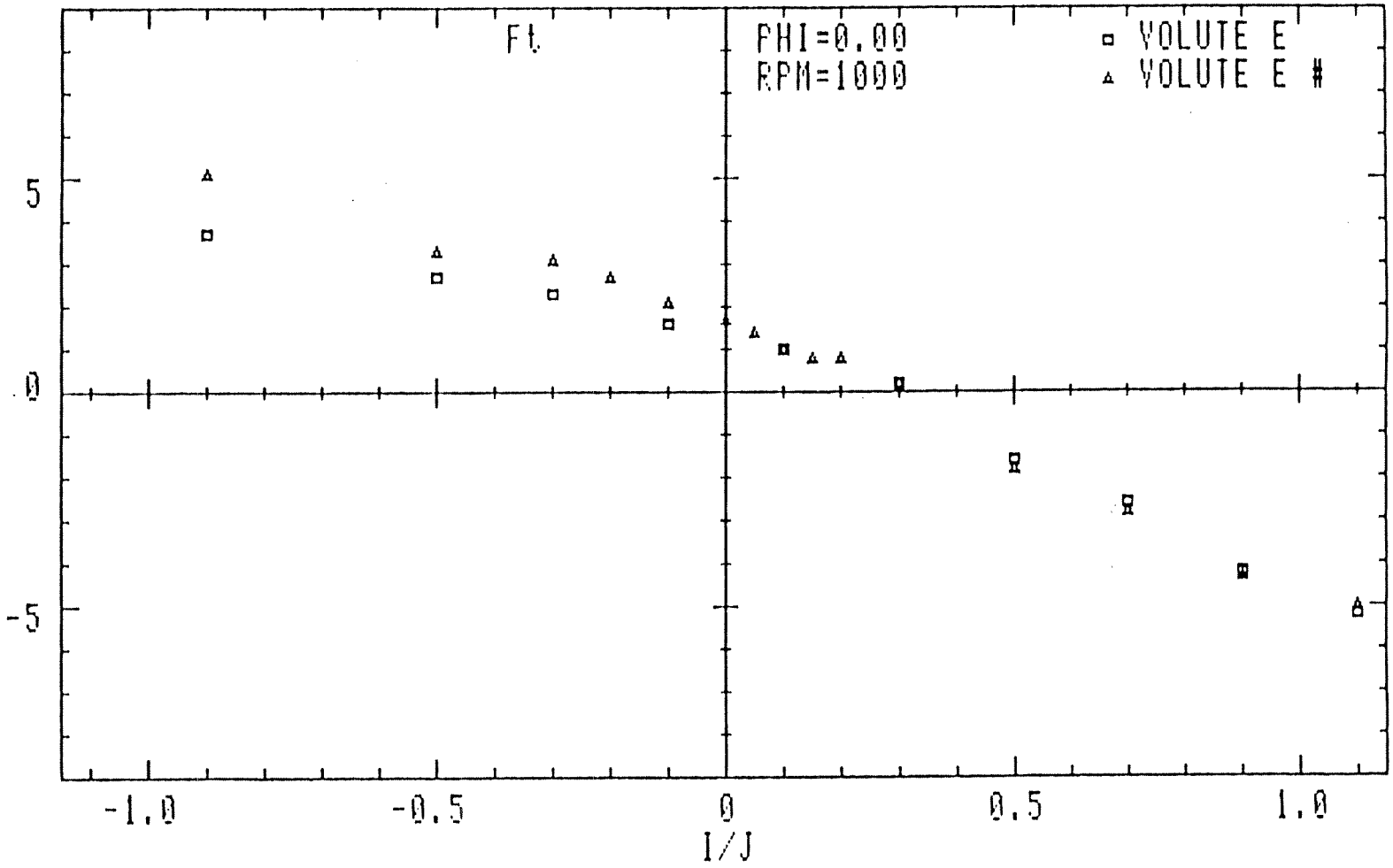
Ft
PHI=0.00
RPM=1000
VOLUTE E
VOLUTE E #
5
0
-5
-1.0
-0.5
0
0.5
1.0
I/J